Spheroplexes: Hybrid PLGA-cationic lipid nanoparticles, for in vitro and oral delivery of siRNA

Danielle Campiol Arruda, Anne-Marie Lachagès, Hélène Demory, Guillaume Escriou, René Lai-Kuen, Pierre-Yves Dugas, Céline Hoffmann, Stéphanie Bessoles, Guillaume Sarrabayrouse, Angelo Malachias, et al.

Spheroplexes: hybrid PLGA-cationic lipid nanoparticles, for in vitro and oral delivery of siRNA

Danielle Campiol Arruda[a,b]*[1], Anne-Marie Lachagès[a], Hélène Demory[a], Guillaume Escriou[a], René Lai-Kuen[c], Pierre-Yves Dugas[d], Céline Hoffmann[a], Stéphanie Bessoles[a], Guillaume Sarrabayrouse[a], Angelo Malachias[e], Stéphanie Finet[f], Pedro Lana Gastelois[g], Waldemar Augusto de Almeida Macedo[g], Armando da Silva Cunha Jr[b], Pascal Bigey[a,h], Virginie Escriou[a]

[a] Université de Paris, CNRS, INSERM, UTCBS, F-75006 Paris, France

[b] Faculdade de Farmácia, Universidade Federal de Minas Gerais, 31270-901 Belo Horizonte, MG, Brazil

[c] Cellular and Molecular Imaging Facility US 25 Inserm- UMS 3612, Faculté de Pharmacie, Université de Paris, F-75006 Paris France

[d] Université de Lyon, Université Claude Bernard Lyon 1, CPE Lyon, CNRS, UMR 5128, Laboratoire Catalyse, Polymérisation, Procédés et Matériaux (CP2M), 69616 Villeurbanne, France

[e]Departamento de Física, Universidade Federal de Minas Gerais, 31270-901 Belo Horizonte, MG, Brazil

[f] Sorbonne Université, IMPMC, CNRS, MNHN, F-75005 Paris, France

[g] Centro de Desenvolvimento da Tecnologia Nuclear, CDTN, 31270-901, Belo Horizonte, MG, Brazil

[h] PSL University, ChimieParisTech, F-75005 Paris, France

* corresponding author: Dr. Danielle CAMPIOL ARRUDA

Keywords: RNA interference; lipoplexes; hybrid nanoparticle; delivery system; biodegradable polymer; oral delivery

[1] Present address: UMR 5305 – Laboratoire de Biologie Tissulaire et d'Ingénierie Thérapeutique, Institut de Biologie et Chimie des Protéines, CNRS/Université Claude Bernard Lyon 1, 7 passage du Vercors, 69367 Lyon cedex 07, France, Tel: 33 4 78 77 71 99/ 33 4 72 72 26 90, danielle.campiol-arruda@univ-lyon1.fr

Abstract:

Vectorized small interfering RNAs (siRNAs) are widely used to induce gene silencing. Among the delivery systems used, lipid-based particles are the most effective. Our objective was the development of novel lipid-polymer hybrid nanoparticles, from lipoplexes (complexes of cationic lipid and siRNAs), and poly (lactic-co-glycolic acid) (PLGA), using a simple modified nanoprecipitation method. Due to their morphology, we called these hybrid nanoparticles Spheroplexes. We elucidated their structure using several physico-chemical techniques and showed that they are composed of a hydrophobic PLGA matrix, surrounded by a lipid envelope adopting a lamellar structure, in which the siRNA is complexed, and they retain surface characteristics identical to the starting nanoparticles, i.e. lipoplexes siRNA. We analyzed the composition of the particle population and determined the final percentage of spheroplexes within this population, 80 to 85% depending on the preparation conditions, using fluorescent markers and the ability of flow cytometry to detect nanometric particles (approximately 200 nm). Finally, we showed that spheroplexes are very stable particles and more efficient than siRNA lipoplexes for the delivery of siRNA to cultured cells. We administered spheroplexes contain siRNAs targeting TNF-α to mice with ulcerative colitis induced by dextran sulfate and our results indicate a disease regression effect with a response probably mediated by their uptake by macrophages / monocytes at the level of lamina propria of the colon. The efficacy of decreased level of TNF-α in vivo seemed to be an association of spheroplexes polymer-lipid composition and the specific siRNA. These results demonstrate that spheroplexes are a promising hybrid nanoparticle for the oral delivery of siRNA to the colon.

1. Introduction

The discovery of RNA interference endogenous pathway [1] and the identification of gene silencing mediated by synthetic small interfering RNA (siRNA) in mammalians cells [2] drew considerable attention to the potential therapeutic application of this type of nucleic acids in the last decades. SiRNA is a 19–21 bp double-stranded RNA which is recognized by a multi-protein nuclease complex called RNA-induced silencing complex (RISC) located in the cytoplasm. The Argonaute (Ago2) nuclease in RISC unwinds siRNA double strand giving rise to the removal of the sense "passenger" strand while antisense "guide" strand remains bound to the complex. The "guide" strand allows RISC to recruit the complementary messenger RNA (mRNA), and thus directs the RISC nuclease to it, triggering its sequence-specific degradation and target gene silencing. The therapeutic use of siRNAs has become an indisputable reality since the launch in 2018 of the first siRNA-based drug, Onpattro®, approved by US Food and Drug Administration (FDA) and European Commission for the treatment of the polyneuropathy caused by hereditary transthyretin-mediated amyloidosis in adults [3,4]. In 2020, the second siRNA-based drug, Givosiran, was approved by the FDA for the treatment of adults with acute hepatic porphyria [5], followed by a third one, Lumasiran [6]. Currently, several clinical trials using siRNA-based drugs are underway [7-8].

siRNA-based therapies have been successfully developed after overcoming some challenging aspects related to the nucleic acid physico-chemical properties and physiological conditions. Naked and unmodified siRNA is a high molecular weight polyanionic hydrophilic molecule. Therefore, siRNA has a low intrinsic membrane permeability which is a major obstacle to overcome in order to achieve efficient cellular uptake. Another obstacle is the short half-life of siRNA due to degradation by nucleases present in the blood and the gastrointestinal tract [7,9]. Finally, the recognition of siRNA as a foreign molecule by Toll-like receptors (TLR) induces an immunostimulatory response that could trigger off-target side effects when administrated *in vivo* [10,11]. The design of siRNA delivery systems is one of the widely used strategies to overcome these barriers in order to improve the stability and cellular uptake of nucleic acids, and to promote their endosomal escape. Due to its negative charge, the siRNA molecule can easily complex with positively charged materials through electrostatic interaction. Cationic lipids and polymers are the most commonly molecules applied for nanoparticles formulations and siRNA vectorization [8,12]. The addition of polyethyleneglycol (PEG) to the surface of delivery systems is achieved by incorporating PEG-conjugated lipids or polymers, which make these delivery vectors more hydrophilic and less likely to be cleared by reticulo-endothelial system (RES). However, the stealth properties of PEG could prevent the interaction between nanoparticles and cell membrane, thereby reducing siRNA delivery [13].

Among the different nanovectors, lipoplexes are well-known and efficient lipid nanoparticles used in the delivery of siRNA [7]. They are positively charged multilamellar nanoparticles, self-assembled due to the electrostatic interaction between anionic siRNA and cationic lipid [14]. In order to promote endosome membrane disruption and siRNA release in the cytoplasm, fusogenic phospholipids, such as 1,2-dioleoyl-sn-glycero-3-phosphoethanolamine (DOPE), are also included in lipoplexes. Unlike the more recently described types of lipid-based nanoparticles, lipoplexes contain only a small number of components, are easy and quick to prepare in aqueous buffer in one step, without any long-lasting or sophisticated process such as dialysis or microfluidics [13]. However, lipoplexes can have drawbacks, such as high cytotoxicity related to the positive charge of cationic lipids [15], as well as low structural stability that can lead to the release of siRNA before it reaches its site of action. Regarding cationic

polymers used in siRNA delivery systems, synthetic polyethyleneimine (PEI) is the most widely used, followed by dendrimers, polyamines, natural polymer chitosan and cyclodextrins. It is also thanks to the electrostatic interaction between opposite charges that are formed anionic siRNA / cationic polymer complexes named polyplexes [7,8,16]. As with lipids, the cationic nature of polymers presents safety concerns. After release of siRNA, free cationic polymers can interact with cellular components and interfere with normal cellular processes and modify gene expression profiles [15,17]. In addition to cationic polymers, poly(lactic-co-glycolic acid) (PLGA), a biocompatible, biodegradable and non-toxic polymer, is widely used for clinical application in drug delivery systems [18-20]. Due to its hydrophobic nature, PLGA forms rigid nanoparticles, with high stability and endocytosis rate. However, hydrophilic molecules such as nucleic acid are encapsulated with low efficiency in PLGA nanoparticles. Moreover, acidic end group of PLGA could decrease or prevent electrostatic complexation with siRNA molecules [19]. One approach used for siRNA vectorization is the assembly of PLGA with cationic molecules such as lipids into hybrid nanoparticles called Polymer-Lipid Hybrid Nanoparticles (PLHNP) [21].

Polymer-lipid hybrid nanocarriers have been proposed to resolve the limitations associated with either polymeric NPs or their lipid counterparts. The structure of these nanoparticles includes a lipid shell which confers biocompatibility, while a polymer core provides stability and controlled release of the drug [21]. PLHNPs have been used as drug or nucleic acid delivery systems for therapy as well as imaging agent for diagnosis purposes [22-26]. Although PLHNPs have been widely studied for systemic administration in cancer therapy [27], their versatility also allows for efficient drug or nucleic acid delivery when administrated noninvasively, such as by oral or pulmonary route [27-29]. A recent review of therapeutic RNA administration by inhalation presented some examples of siRNA delivery with PLHNPs [30]. Due to their physicochemical stability, PLHNPs also have promising advantages for oral drug administration [28, 31]. Although siRNA therapies targeting gastrointestinal diseases have been widely studied, there is no publication reporting oral administration of siRNA-PLHNPs [32]. The structural organization of PLHNPs depends on their method of preparation, which can be carried out using one- or two-step approaches (recently reviewed in [21,27]). Regarding the one-step approach, nanoprecipitation is a well-known method used for the encapsulation of hydrophobic drugs in polymeric particles and PLHNPs [27,33]. In this process, a hydrophobic polymer dissolved in an organic water-miscible solvent is added dropwise in an aqueous phase under stirring triggering the self-assembly of the polymer and the spontaneous nanoparticle precipitation. Some advantages of this method are: (i) use of a solvent of low toxicity according to the ICH guideline for residual solvents Q3C(R6), (ii) mixing at low energy, (iii) narrow dispersion of nanoparticle size and (iv) no surfactant required [34]. However, the major drawback of this method is the low efficiency of encapsulation of hydrophilic drugs, such as nucleic acids. Although many studies investigating the use of PLHNP to vectorize siRNA have been reported, few groups have used nanoprecipitation as a method to obtain efficient PLHNPs for siRNA delivery [35-38].

In this study, the objective was the development of novel hybrid lipid-polymer nanoparticles from siRNA lipoplexes using a simple modified nanoprecipitation method. With this method, we succeeded in preparing hybrid lipid-polymer nanoparticles, stable and efficient for the delivery of siRNA and specific silencing of target gene. Because of their morphology, we called them Spheroplexes (Sphx). An in-depth physicochemical characterization of the spheroplexes was carried out to elucidate their structure, the organization of their components and to assess the complexation of siRNA within the particles. We also analyzed the different types of particles, as well as their

frequency, found in the final preparation. Finally, we showed that spheroplexes are suitable for oral administration since when they were administered, without inducing significant toxicity, by oral gavage to mice with ulcerative colitis, a regression of the disease could be observed if the administered spheroplexes contained TNF-α specific siRNAs.

2. Materials and methods

2.1. Materials

siRNAs (unmodified) specific to luciferase (sense strand, 5' CUU ACG CUG AGU ACU UCG AdTdT 3'), mouse TNF-α ($siRNA_1$, sense strand, 5' GAC AAC CAA CUA GUG GUG CdTdT 3'; $siRNA_2$ sense strand, 5'GGU UCU CUU CAA GGG ACA AdTdT 3') or non-silencing siRNA used as negative control (sense strand, 5' UUC UCC GAA CGU GUC ACG UdTdT 3') or fluorescent (non-silencing siRNA modified at the 5' end of the sense strand with Alexa® 488 or Alexa® 647) were obtained from Eurogentec (Seraing, Belgium). DOPE (1,2-dioleoyl-sn-glycero-3-phosphoethanolamine) was obtained from Avanti Polar Lipids (Coger SAS, Paris, France). Sodium alginate (reference 180947) and poly(lactic-co-glycolic acid) (PLGA, ester terminated) with lactic/glycolic monomer composition ratio of 50:50 (Mw 24,000-38,000 Da) or 85:15 (Mw 50,000-75,000 Da) were purchased from Sigma-Aldrich (St. Quentin Fallavier, France). Fluorescent PLGA, poly(lactide-co-glycolide)-FPR648, 50:50 FPR648 fluorescent endcap, Mw 10,000-25,000 Da was obtained from PolySciTech (Akina Inc., West Lafayette, USA). DSS (Dextran Sodium Sulfate, 36 000-50 000, colitis grade) was obtained from MP Biomedicals (Illkirch, France).

2.2. Preparation of siRNA lipoplexes (Lpx)

Cationic liposomes were prepared from cationic lipid DMAPAP (2-{3-[Bis-(3-amino-propyl)-amino]-propylamino}-N-ditetradecylcarbamoyl methyl-acetamide) [39] and zwitterionic lipid DOPE (1/1, M/M) at 20 mM in H_2O as previously described [40]. Lipoplexes (+/- R8) were prepared by mixing an equal volume of a solution, containing siRNA (luciferase or control) and sodium alginate (ratio 1/1, w/w) diluted in 150 mM NaCl, and a dispersion of cationic liposome also in 150 mM NaCl, and rapidly mixed by vortexing. Lipoplexes were allowed to form at least for 30 min at room temperature (RT) before use. The +/- charge ratio (+/- R) was calculated using the molar ratio of positive charges (3 positive charges per molecule of DMAPAP) and the molar ratio of negative charges (3.03 and 5.05 nmoles of negative charges/mg of siRNA and sodium alginate, respectively). Fluorescent lipoplexes were prepared under the same conditions, but using a siRNA coupled to Alexa® 488 or or Alexa® 647.

2.3. Preparation of siRNA spheroplexes (Sphx)

A solution of PLGA (PLGA concentration 2 or 5 µg/µL) in acetone was added to a dispersion of lipoplexes (siRNA concentration 6 µM) prepared as described above. Spheroplexes were formed by two sequential additions of a volume of the PLGA solution (at the indicated concentration) in acetone, corresponding to half the volume of the dispersion of lipoplexes (FIG.S1A). Each addition of PLGA was followed by the evaporation of acetone under reduced pressure. Spherosome (FIG.S1B) and PLGA particles (FIG.S1C) were prepared according to the same protocol, replacing the dispersion of lipoplexes with a dispersion of liposomes or with saline solution, respectively. Fluorescent particles

were prepared under the same conditions, but using either fluorescent lipoplexes (with Alexa® 488 or Alexa® 647 labelled siRNA), or fluorescent PLGA (FPR648-PLGA), or both. For sample preparation for SAXS experiments, the steps were the same but higher concentrations were used (lipoplexes dispersion, 25 µM siRNA, PLGA 6.7 µg/µl).

2.4. Size and ζ potential measurements

Size and ζ potential measurements were performed on a MALVERN Zetasizer Nanoseries Nano ZS. Particles dispersions were prepared in 100 µl of NaCl 150 mM with a final concentration of siRNA of 334 nM. For ζ potential measurements, particles (siRNA 33 nM) were prepared in 15 mM NaCl.

2.5. Small-angle X-ray scattering (SAXS)

SAXS measurements were carried out at the SWING beamline of SOLEIL (Gif-sur-Yvette, France), using a fixed energy of 12.0 keV. A PCCD170170 (AVIEX) 2D detector was placed at a 1.5 m distance from the sample, covering a momentum scattering vector (Q) range that spans from 0.0075 until 0.8 $Å^{-1}$. In this setup a resolution of 0.00067 $Å^{-1}$ is achieved. All measured scattering patterns are angularly isotropic in this work. Hence, our datasets are shown after an angular integration of the detector area (commonly referred as ‘‘cake”), averaged and background subtracted using FOXTROT program (V3.4.1, Xenocs). Particles dispersions prepared in 100 µl NaCl 150 mM with a final concentration of siRNA of 25 µM were inserted manually into a capillary. Ten to sixty frames were recorded with an acquisition time from 10 to 300 msec depending on sample concentration and signal to noise-ratio.

2.6. Atomic Force Microscopy (AFM)

AFM experiments were carried out using the MFP-3D Classic microscope (Asylum Research). Measurements were taken in tapping mode, recording height and phase images. Particles dispersions were diluted in water, dripped on silicon wafers and dried under vacuum overnight. The microscope operated at room temperature and images were acquired with a silicon tip-cantilever (tip diameter < 10 nm) with a stiffness of 4.5 (2.5-8.5) N m^{-1} and a resonance frequency around 150 kHz. All samples were analyzed with a scan rate of 0.5-1.0 Hz and the data were obtained in a moderate force mode with set point amplitude adjusted to 60-70% of the free air amplitude. Height mode was used for image analysis using Igor Pro 6.34A software.

2.7. Transmission electron microscopy (TEM), Cryo-TEM and Scanning electron microscopy (SEM)

TEM images were performed on a microscope JEOL, JEM 100S. A drop (20 µl) of particles dispersion (siRNA concentration 400 nM) was first applied onto a Formvar/carbon copper grid 200 mesh from Agar Scientific pre-treated with Bacitracine 0.1 % (w/v), allowed to adsorb for 2 min, and blotted with filter paper. A drop of 2% (w/v) aqueous uranyl acetate stain was applied to the sample grid, allowed to stain for 2 min, blotted with filter paper and air drying for 4 min. To prepare ultrathin sections of spheroplexes, pelleted particles were mixed with a positive staining solution of 2% (w/v) of osmium tetroxide (OsO_4) in water for 1h at 4 °C in dark. OsO_4 solution was removed and replaced by successive alcohol baths to dehydrate the samples. They were then embedded in Epon resin which

hardens by polymerization. The resulting blocks were cut with a microtome equipped with a diamond knife to obtain 80 nm thick sections. Finally, sections were put on a carbon-coated copper grid for their observation. The particles dispersions were observed by cryo-TEM in order to preserve their morphology. 3 µL of the dispersion was deposited onto a 300 mesh Lacey carbon film grid (EMS) and quench-frozen in liquid ethane using a Thermo Fisher Vitrobot. Samples were transferred in the microscope (JEOL 1400F - LaB6, Centre Technologique des Microstructures (CTµ) – University Claude Bernard Lyon 1, Villeurbanne, France) using a precooled cryo-transfer holder (Fischione 2550) and observed with a Gatan Rio16 camera at an accelerating voltage of 120 kV in low-dose conditions. SEM images were performed on a Scanning Electron Microscope (Jeol JSM-6510 LV). Particles dispersions were deposited for 2 min on a Formvar carbon film on copper grids bonded on aluminum mount by carbon adhesive tabs, blotted with filter paper and air drying for 20 min at RT. The samples were covered with metal layer (Jeol JFC-1300 auto fine coater), observed at 10 Kv and photographed at different magnifications.

2.8. X-ray photoelectron spectroscopy (XPS)

XPS analysis was performed on a Specs surface analysis system equipped with a Phoibos 150 electron analyzer using a monochromatized Al Kα radiation (1486.6 eV) at a power of 350 W. An electron flood gun operating at 0.1 µA was used to compensate the charge effect in the samples and the C 1s signal (284.6 eV) was employed as reference for the calibration of the binding energies (BE) of different elements. CasaXPS software was used to process the analysis data and to estimate the samples surface atomic concentrations. Lipoplexes and spheroplexes were prepared at final siRNA concentration of 6 µM. Polymeric solution in acetone were prepared at PLGA concentration of 5 µg/µl. The sample preparation for XPS analysis required the fixation of particles dispersions or PLGA solution on the sample holder slides using graphite adhesive tape and consecutive steps of drop drying in the desiccator until obtaining a thick and stable film over the tape.

2.9. Electrophoresis on acrylamide gels

Lipoplexes and spheroplexes were prepared as described above. Samples were either let untreated or particles were dissociated by addition of Triton X-100 (final concentration 20 or 30%) and NaCl 1M, and heating at 37 °C for 10 min. Before loading on 6% acrylamide gels (TBE-Urea, Invitrogen), TBE-urea sample buffer 2× (Invitrogen) was added. Electrophoresis was performed in TBE running buffer at 180 V for 30 min. Gels were put into a SYBR® Green II bath (1/10,000) for 30 min and the stained siRNA bands were visualized on an ultraviolet transilluminator and digitalized. An amount of 0.3 µg siRNA per lane was used.

2.10. Analysis of particle distribution using flow cytometry

Fluorescent or non-fluorescent lipoplexes and spheroplexes were prepared as described above and diluted in filtered PBS (cut-off 0.2 µm) before analysis on a Guava Easycyte™ cytometer (Millipore) equipped with two lasers (excitation 488 nm and 642 nm, respectively).

2.11. Gene silencing and cellular viability on cultured cells

B16-Luc were obtained and transfected as described [40,41]. Lipoplexes or spheroplexes dispersions were diluted in complete culture cell medium (siRNA concentration as indicated) and added to cells for 24 h in 24-well plates. Transfection medium was replaced by fresh medium for another 24 h, then the transfected cells were washed twice with PBS and lysed, and luciferase and total protein were assayed as in [40]. The results, calculated in cps (count per second), were normalized to the total protein concentration of each sample and the gene silencing efficacy was expressed as the luciferase activity inhibition percentage relative to the luciferase activity of non-transfected control cells. Cellular viability was assayed on transfected B16-Luc cells as described above, using the MTT test as described [42].

2.12. In vivo experiment

All animal experiments were performed in accordance with the guidelines of Directive 2010/63/EU and approved by the Ethics Committee for Experimentation of Université de Paris and authorized by the French Ministry of National Education, Higher Education and Research (APAFIS# 20157-2018041117244146v4). Mice were housed in a temperature- and humidity-controlled room with a 12-h day/12-h night cycle and had free access to water and food. Male C57Bl/6 mice (7 weeks) were purchased from Janvier Labs. Acute colitis was induced in mice by addition of 4% (w/w) DSS (MW 36,000–50,000) in their drinking water for the duration of the study, while control group received regular tap water. Mice were monitored every day for their health condition. From day 1 to day 6, mice were given saline, or lipoplexes or spheroplexes (prepared with PLGA 5 µg/µl) loaded with control or TNF-α siRNA (1 mg/kg body weight in 200 µl final volume) by oral gavage using a blunt-tipped feeding needle inserted into the esophagus. At day 7 mice were sacrificed, blood was collected and the large intestine was surgically removed and carefully washed with PBS. Samples of the median part of the large intestine were homogenized in lysis buffer (100 mM TRIS, pH 7.4; 1 mM EDTA; 150 mM NaCl; 1% (v/v) Triton X-100; 0.5% (w/v) Sodium Deoxycholate), supplemented with proteinase inhibitor, at the rate of 10 µl/mg of colon sample, using Soft tissue homogenizing CK14 tubes (Ozyme) and Precellys Evolution homogenizer (Bertin Instruments) to extract the proteins from the tissue samples. Protein containing supernatant was separated by centrifugation at 13,000 g for 10 min at 4 °C and stored at −70 °C until analysis. Cytokines levels were assayed using ELISA kits (DuoSet ELISA for mouse TNF-α, IL-6, IL1-β, IFN-γ, CCL2/JE/MCP-1 and CXCL1/KC from R&D Systems) according to the manufacturer's protocol and normalized against the total protein content of each individual sample as determined by bicinchoninic acid assay (Pierce). Values are expressed as picogram (pg) of murine cytokine expressed per mg of total protein content of each sample. Chemokine KC level was also assayed on serum and the values are expressed as pg of cytokine per ml of serum. Plasma biomarker assays were performed with an Olympus AU 400 multiparameter, in the Biochemistry Platform of Centre de Recherche sur l'Inflammation (CRI) CNRS - UMR 1149 Université Paris Diderot.

2.13. In vivo toxicity experiment

Mice under normal diet were given saline, or lipoplexes or spheroplexes (prepared with PLGA 5 µg/µl) loaded with control unlabeled or Alexa 647 labeled siRNA (1 mg/kg body weight in 200 µl final volume) by oral gavage. At day 1 or at day 7 mice were sacrificed, spleen, heart and the large intestine were collected, and weighted. Blood was collected in 15 µL of EDTA the day of sacrifice to

perform a Complete Blood Count (CBC). White Blood Cell (WBC), Red Blood Cell (RBC), hematocrit (HCT), Hemoglobin, platelet (PLT), lymphocytes, monocytes, granulocytes, Mean Corpuscular Hemoglobin Concentration (MCHC), plateletcrit (Pct), Mean Corpuscular Volume (MCV), were measured using digital cell counter (MS9-5s -Melet). Cytokines levels were assayed on colonic lysates and plasma biomarker assays were performed as described above (2.12).

2.14. Biodistribution experiment

Colonic tissues dissociation and staining. First, the colonic tissues were washed in DTT buffer (HBSS medium (Gibco, ref: 14170-088), FCS 2.5%, Penicillin-Streptomycin (50 U/mL), Gentamicin (0.05 g/L), DTT (5 mmol/L)) during 8 min at 37 °C on a shaking plate (150 rpm) and then, the lamina propria (LP) was separated from the epithelium following 3 incubations (8 min, 37 °C, 150 rpm) in an EDTA buffer (HBSS, FCS 2.5%, Penicillin-Streptomycin (50 U/mL), Gentamicin (0.05 g/L), EDTA (5 mmol/L)). LP samples were washed with a Hepes buffer (HBSS, HBSS, Penicillin-Streptomycin (50 U/mL), Gentamicin (0.05 g/L), Hepes (1 mM)) and minced into 1-mm^2 fragments before incubation during 30 min with shaking in a dissociation solution containing enzymes (HBSS, FCS 1.2%, Penicillin-Streptomycin (50 U/mL), Gentamicin (0.05 g/L), Dispase (50 g/L), Collagenase (40 g/L) and DNAse (1 g/L)). Mucus and large debris were removed by filtration through a 40 µm cell strainer (BD). After centrifugation of the cell suspension, the pellet was taken up in 5mL of complete medium (RPMI-1640 (Gibco; ref: 61870-010), FCS 10%, Penicillin-Streptomycin (50 U/mL), Gentamicin (0.05 g/L)) and the cells were counted. Antibodies staining were performed on $2x10^6$ cells from the colonic cell suspension. Cells were washed with PBS and incubated with the viability marker (ebioscience, ref: 65-0866-18) (30 min at 4 °C). After washing with PBS, they were incubated for 30 min at 4 °C with the antibody mix composed of following antibodies: Anti-mouse CD45-PE (Miltenyi, ref: 130-102-596); Anti-mouse MHC-II (Biolegend, ref: 107626); Anti-Mouse CD19 Brillant Violet 605 (Biolegend, ref:115540); Anti-Mouse CD3 Brillant Violet 785 (Biolegend, ref: 100232); Anti-Mouse CD11b AF700 (Biolegend, ref: 101222); Anti-Mouse CD11c Brillant Violet 711 (Biolegend, ref: 117349); Anti-Mouse Ly6G FITC (Miltenyi, ref: 130-102-296); Anti-Mouse Ly6c FITC (BD, ref: 560596) ; Anti-Mouse CD16/CD32 (ebioscience, ref: 14-0161-85). After incubation, cells were washed with flow cytometry buffer (PBS, FCS 2%, 2 mM EDTA) and fixed for 20 min at RT with the cytofix/cytoperm solution (Invitrogen, ref: 00-5223-56).

Blood cell content staining. Around 150 µl of blood were collected directly in presence of 15 µL of EDTA (0.5 M). After CBC, Red blood cells were lysed with a hypotonic solution of ACK (Ammonium-Chloride-Potassium: 150 mM NH_4Cl; 10 mM $KHCO_3$; 0.1 mM EDTA, pH 7.2-7.4) for one minute at RT. Blood samples were then washed in DMEM 10% FCS and suspended in the same medium. Cells were washed with PBS and incubated for 20 min at 4 °C in 30 µL of a solution of Zombie UV™ Fixable Viability Kit (biolegend, ref: 423107). After washing with PBS, cells were stained during 30 min at 4 °C with a mix of antibodies containing : anti-CD16/32 (thermoFisher, ref: 16-0161-86), Anti-mouse CD45-PE (Miltenyi, ref: 130-102-596); Anti-mouse MHC-II (Biolegend, ref: 107626); Anti-Mouse CD11b AF700 (Biolegend, ref: 101222); Anti-Mouse CD3 Brilliant Violet711 (biolegend, ref: 100241); Anti-Mouse CD19 Brilliant Violet 711 (biolegend, ref: 115555), Anti-Mouse NK1.1 Brilliant Violet711 (biolegend, ref: 108745); anti-Mouse Ly6C-APC-Cy7 (BD: ref 560596). Cells were washed in flow cytometry buffer (PBS, 2% FCS, 2 mM EDTA) and fixed for 20 min at RT with the cytofix/cytoperm solution (Invitrogen, ref: 00-5223-56).

Cytometry analysis. After a final wash, the cells were suspended in flow cytometry buffer and analysed in a Fortessa cytometer (BD). Staining analysis was performed using Flowjo software.

2.15. Statistical analysis

All results were analyzed with the unpaired non-parametric Mann-Whitney test using two-tailed P-values. Results with $p < 0.05$ were considered statistically significant.

3. Results

3.1. Preparation and physico-chemical characterization of Spheroplexes, PLGA-based hybrid nanoparticles, prepared by nanoprecipitation from a dispersion of lipoplexes

3.1.1. Formulation parameters

PLGA-lipid hybrid nanoparticles were prepared following a modified one-step nanoprecipitation method. The specificity of the one-step method we propose is based on the use, as aqueous phase, of a dispersion of siRNA lipoplexes in saline solution and, as organic phase, of a solution of PLGA in acetone, without addition of surfactant or use of high temperature (Fig.S1A). Indeed, since phospholipids have a recognized surfactant effect [43], and we prepared siRNA lipoplexes at high +/- charge ratio, i.e. with an excess of lipids, we assumed that these excess lipids could play the role of stabilizer and allow the conversion of lipoplexes into PLHNPs with a strong complexation of siRNA. We used a dispersion of siRNA lipoplexes, (patented in [44]) which exhibit enhanced gene silencing efficiency and based on the self-assembly of siRNA, a cationic liposome composed of equimolar amounts of DOPE and DMAPAP (synthesized as in [39]), and an anionic polymer [40,41]. Several types of PLGA, varying according to the type of terminal group and the lactide:glycolide molar ratio, are available. The ester-terminated PLGA, which exhibits a neutral charge, has been preferred over the acid form, in order to reduce electrostatic interactions with cationic lipids, and to ensure the formation of a polymer core. The lactide: glycolide molar ratio, which determines the degradability of the polymer as well as its mechanical resistance [45], is correlated with the stability of the PLGA nanoparticles. We decided to use PLGA with monomer molar ratio of 50:50, which presents the faster biodegradation rate, or 85:15.

We first miniaturized the one-step nanoprecipitation method to adapt it to the low working volume (a few microliters). To replace the dropwise addition usually performed in the conventional nanoprecipitation process, the PLGA solution was added to the lipoplex dispersion all at once, or split and added in two or in five steps. The first condition has been set aside, since we observed the formation of a large white pellet, a sign of precipitation of the polymer, in accordance with other study analyzing formulation parameter non-miniaturized nanoprecipitation [46]. The hybrid nanoparticles prepared by adding the volume in two or five fractions exhibited similar physicochemical characteristics. From a practical point of view, the addition in two steps was therefore chosen. The effect of the pH of the aqueous phase on particle formation was also evaluated. The preparation of lipoplexes in isotonic buffered solution at pH 7.4 or in simple isotonic solution (150 mM NaCl, pH ≈ 5.5) made it possible to form nanoparticles with similar morphological

characteristics. With this method, hybrid nanoparticles have been successfully obtained using two types of PLGA, i.e. with a lactide: glycolide molar ratio of 50:50 or 85:15. Although this result suggests that it is possible to obtain delivery systems with potentially adjustable release profiles, the effect of the copolymer ratio will not be presented here but will be explored in future studies.

Thereafter, the method of preparing the hybrid particles was defined as follows: two-step addition of a solution of PLGA 50:50 (5 µg/µl) in a dispersion of siRNA lipoplexes prepared in an isotonic solution of pH 5.5. In order to assess whether a modification of the PLGA concentration could influence the physico-chemical characteristics and homogeneity of the formulation, we also prepared hybrid particles with a solution of PLGA at 2 µg/µl.

3.1.2. Morphology and physico-chemical characterization

First, we examined the morphology of the obtained PLGA-based hybrid nanoparticles. As can be seen in FIG.1, using both SEM (FIG.1A-B) and AFM (FIG.1E), the PLGA-based hybrid particles appeared clearly spherical, unlike lipoplexes (FIG.1D and FIG.1F) which presented various shapes, more or less rounded. Because of their noteworthy spherical shape, we chose to name these new particles spheroplexes (Sphx). The particles studied will therefore be noted Lpx for lipoplexes, Sphx 2 and Sphx 5 for spheroplexes prepared with a solution of PLGA of concentration at 2 and 5 µg/µl, respectively. The spherical morphology exhibited by Sphx was close to the perfectly spherical form presented by a particle of PLGA (FIG.1C). Sphx also exhibited a surface that appeared more homogeneous than that of Lpx (compare FIG.1E and FIG.1F).

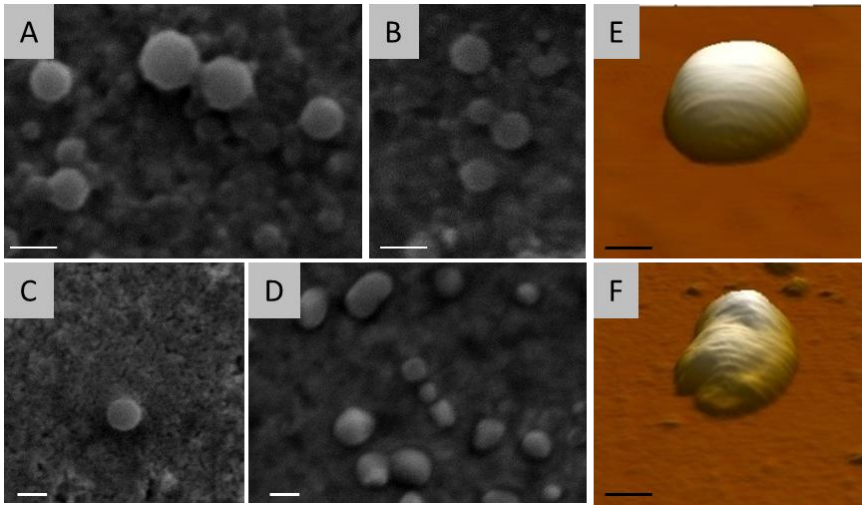

Fig. 1. SEM micrographs of Sphx 5 (A, B), PLGA nanoparticles (C) and Lpx (D) after coating with metal layer. The scale bar is fixed to 1 µm. 3D AFM images of Sphx 5 (E) and Lpx (F). The scale bar is fixed to 100 nm.

The physico-chemical properties of Lpx and Sphx are presented in Table 1. Sphx exhibited a larger hydrodynamic diameter than Lpx, with a higher polydispersity index (PDI), independently of the concentration of PLGA. However, a positive ζ potential was maintained in both Sphx formulations, suggesting the presence of cationic lipid on the surface of the hybrid nanoparticles.

Table 1- Physico-chemical properties of particles. Results denote mean ± SD (n= 3).

	Size (nm)	PDI	ζ Potential (mV)
Lpx	182 ± 9	0.295 ± 0.049	+ 59 ± 15
Sphx 2	345 ± 2	0.414 ± 0.018	+ 62 ± 1
Sphx 5	291 ± 24	0.352 ± 0.015	+ 57 ± 4

We also examined the particles using TEM. Lpx appeared as particles of quite various shapes, with condensed multi-lamellar structures exhibiting several concentric lamellae or a more confuse arrangement in which clearly visible lamellae were detected (FIG.2A). These structures are characteristic of Lpx [14]. Sphx presented a very different aspect from that of Lpx since they exhibited a more regular, spherical shape, composed of a white inner part and a gray corona (FIG.2C). This morphology was close but not identical to that of nanoparticles of PLGA (FIG.2B). Indeed, PLGA nanoparticles appeared as a perfectly spherical white particle with no gray corona. We simply noticed a homogeneous black shadow due to deposition of contrast agent at the surface of PLGA nanoparticles.

Regardless of the concentration of PLGA used, Sphx were characterized by a gray corona of variable thickness and an inner part on which tangled linear forms appeared (FIG.2C and Fig.S2A-B). Equivalent but less regular particles (FIG.S2C) can also be prepared by replacing the dispersion of Lpx with a dispersion of liposomes before addition of PLGA, forming what we called “spherosomes” (FIG. S1B). By comparison of the morphology of Sphx and that of PLGA nanoparticles, we can hypothesize that the inner part of Sphx was composed of PLGA but the nature of the corona remained to be determined. We therefore treated Sphx with osmium tetroxide, which is known to stain lipids [47], and then embedded treated Sphx in Epon resin. After polymerization of the resin, we made ultra-thin sections (80 nm) which were then observed using TEM. FIG.2 (D-I) shows particles surrounded by a uniform dark shell, revealing the lipid coating. These results suggest that, when PLGA was added to Lpx dispersion, lipids, originally organized into Lpx, reorganize to form a layer surrounding the PLGA matrix. This lipid reorganization was observed regardless of the concentration of PLGA used to prepare Sphx. In order to complete this structural study, we also performed cryo-TEM analysis of Sphx and Lpx. Cryo-TEM images show that Lpx present typical multilamellar structures with irregular morphology (black arrows in Fig.2J), consistent with structures detected in TEM, SEM and AFM. analysis. A few liposomes (white arrows) and transient forms of lipoplex formation (asterisks) were also observed in the Lpx dispersion (Fig.2J). Sphx were identified as gray nanoparticles with homogeneous high electron density suggesting the presence of PLGA. As shown in Fig.2K, multilamellar lipid bilayers, similar to Lpx, were observed at the border of particles comparable to a shell with variable thickness. Some particles presented a structure like small liposomes or fragment of Lpx in their inner part. Some residual liposomes, lipoplexes and other types of transient nanoparticles, were associated with Sphx as large aggregates in accordance to the high PDI measured by DLS (Table 1).

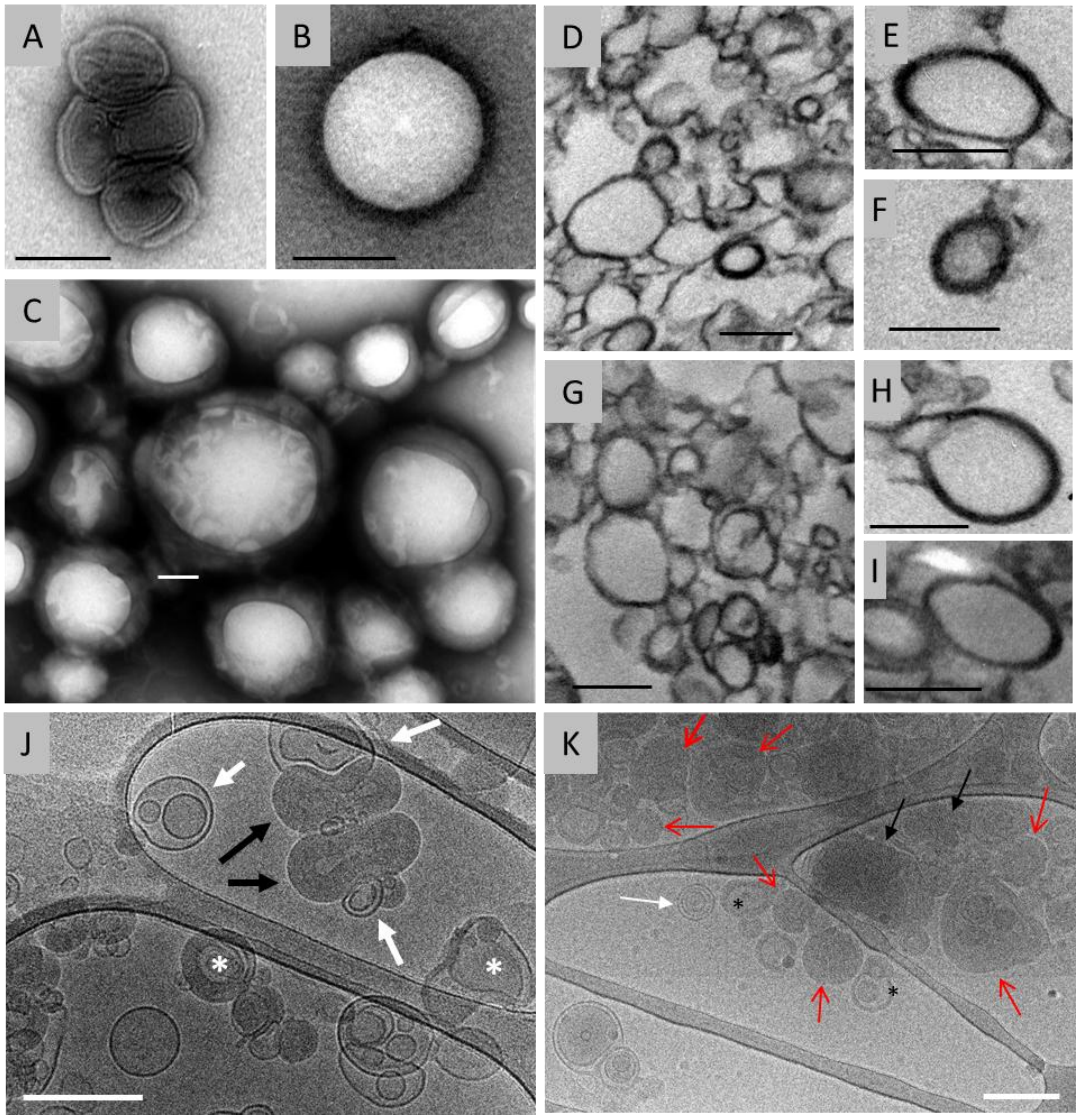

Fig. 2. TEM micrographs of Lpx (A), PLGA particles (B) and Sphx (C) after negative staining with uranyl acetate. TEM micrographs of ultrathin cross sections of Sphx 2 (D-F) and Sphx 5 (G-I). All samples (D-I) were treated with osmium tetroxide solution (2% w/w). Cryo-TEM images of (J) Lpx and (K) Sphx dispersions. Black arrows indicate multilamellar Lpx, white arrows indicate empty liposomesand red arrows indicate Sphx. Asterisks indicate transitory nanoparticles. The scale bar is fixed to (A-C) 100 nm or (D-K) 200 nm.

3.1.3. Structure

In order to understand Sphx structure, we carried out small-angle X-ray scattering (SAXS) to infer the structure of the lipid phase in Sphx. Dispersed in saline solution, Lpx exhibited a mixture of two

phases, cubic and lamellar (FIG.3A, green curve), as we recently showed [41]. In contrast, a dispersion of Sphx presented a single phase (FIG.3A, grey curve). The position of the main peak is in agreement with the packing observed previously for a lamellar phase. As expected, structural peaks are completely absent in a dispersion of PLGA particles, (FIG.3A, blue curve) indicating a lack of supramolecular organization. Interestingly, a dispersion of spherosomes presented a similar mixture of two phases, cubic and lamellar, as the starting dispersion of liposomes (see FIG.S3, in supplementary material), with peak positions slightly shifted towards lower values of q.

A

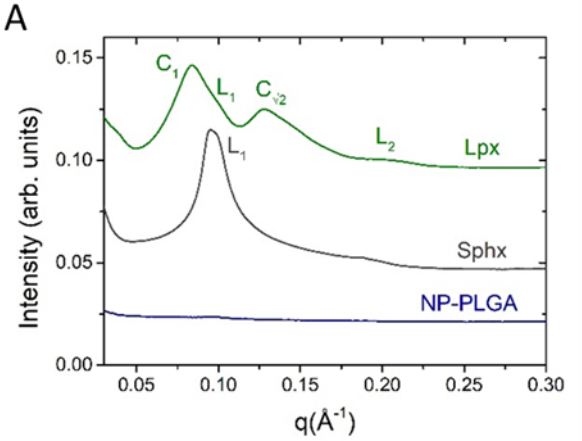

B

Particles	Surface composition (Atom %) O 1s	N 1s	C 1s	P 2p
Liposome	6.4	6.7	80.6	0.8
Lpx	12.5	5.4	74.7	0.8
Sphx 2	13.2	5.1	73.1	0.9
Sphx 5	12.9	5.3	73.6	1.0
NP-PLGA	23.0	n.d.	73.0	n.d.

n.d. not detected

Fig. 3. Structural analysis. (A) SAXS profiles of particles in dispersion in 150 mM NaCl. Lpx (green curve), Sphx 2 (grey curve) and PLGA nanoparticles (NP-PLGA, blue curve). (B) XPS surface elemental composition of particles.

We completed the analysis of Sphx with a characterization of the particle surface using the technique of X-ray photoelectron spectroscopy (XPS), which we have already used to compare the surface of different types of Lpx [41]. The surface composition of Sphx, as obtained from the XPS spectra (data not shown), were compared to those of Lpx, liposome or PLGA in solution (see table of FIG.3B). Sphx 2 and Sphx 5 were found to have a surface composition very close to that of Lpx, but relatively different from that of liposomes. In addition, the surface composition of Sphx was very different from that of PLGA. In particular, PLGA contained neither nitrogen nor phosphorus atoms, while about 5% of the atoms detected on the surface of Sphx was nitrogen, a concentration almost identical to that found at the surface of Lpx.

Taken together, these results confirm that Sphx were nanoparticles composed of a PLGA matrix surrounded by a bilayer of lipids at their surface, adopting a lamellar phase, and whose atomic composition was nearly identical to that of Lpx. When PLGA was added to Lpx dispersion, lipid reorganization occurred. One can however wonder if this lipid reorganization induced a modification of the interaction of siRNAs with lipids and if siRNAs remained associated with this lipid layer or if siRNAs were released. To investigate the association of siRNA with Sphx, we used electrophoresis on urea-acrylamide gels (FIG.4). For this purpose, Sphx or Lpx were loaded onto the gel either intact (untreated), or after dissociation by treatment with detergent, salt and heating, in order to completely disassemble the particles and assess the amount of intact siRNA remaining associated with them. When untreated particles were loaded without previous treatment, only the siRNA molecules not associated with the particles can migrate into the gel.

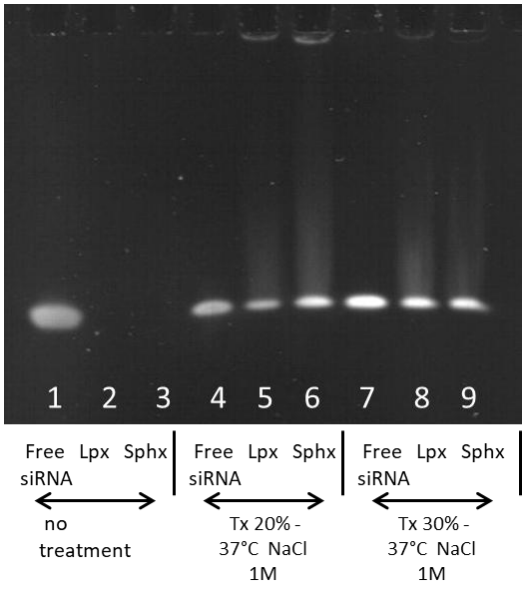

Fig. 4. Association of siRNAs with Sphx assayed by gel retardation assay. Lpx, Sphx and free siRNA were electrophoresed through 6% acrylamide gel and free siRNA was visualized with Sybr Green II. Lpx (2, 5, 8), Sphx (3, 6, 9) or free siRNA (1, 4, 7) were loaded either untreated (1-3) or after treatment with Triton X-100 20% (4-6) or 30% (7-9) at 37 °C in the presence of 1M NaCl. Each well contains 0.3 µg of siRNA.

As expected, no band was detected when untreated Lpx (FIG.4A, lane 2) were loaded onto the gel. As with Lpx, no band was detected when untreated Sphx were loaded on the gel (lane 3), indicating that there was no release of siRNA upon formation of the particles. In addition, siRNA was actually associated with the particles since if we dissociated all the components of the particles, Lpx (lanes 5 and 8) or Sphx (lanes 6 and 9), we recovered the released siRNA, which can migrate freely. It can therefore be concluded that the formation of Sphx did not lead to the release of siRNAs. On the contrary, they remained associated with cationic lipid bilayers, in the corona or inside the the matrix of Sphx.

3.2. Composition of the particle population

Having shown that Sphx were composed of heterogeneous nanoparticles containing the siRNAs, it was important to assess the composition of the particle population dispersed. Indeed, considering the preparation process and the polydispersity, the final dispersion of Sphx was likely to contain also, in addition to Sphx, (i) unmodified Lpx, (ii) PLGA nanoparticles, (iii) liposomes, co-existing in the dispersion of Lpx, and (iv) spherosomes, composed of a PLGA inner part, surrounded by a corona of lipids constituting the liposomes. Taking advantage of the capacity of flow cytometry to analyze particles individually and the possibility of identifying each type of particle by introducing fluorescent components, we first checked whether it was possible to detect, by this technique, the different types of particles listed above and prepared as described in FIG.S1. As shown in FIG.S4, it was possible to detect the lipid particles, such as liposomes and Lpx, as well as PLGA nanoparticles, spherosomes and Sphx. Moreover, if a fluorescent siRNA (siRNA-Alexa 488) was used, it was

observed that the dots of particles moved to areas corresponding to a high level of green fluorescence. Likewise, the use of fluorescent PLGA (PLGA-FPR645) produced the same phenomenon for PLGA nanoparticles, spherosomes and Sphx. Finally, if both fluorescent siRNA and PLGA were used, the different particles potentially present in the preparation of Sphx can be distinguished.

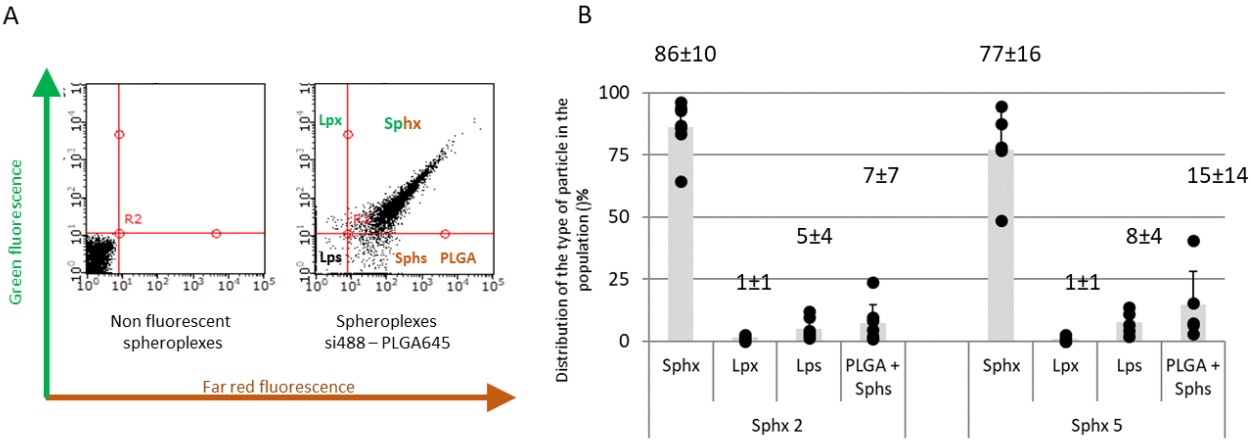

Fig. 5. Flow cytometry analysis of spheroplex dispersion. (A) Representative dual fluorescence dot plot of an unlabeled (left) or double labeled (right) Sphx preparation. Sphx, unlabeled or labeled via incorporation of siRNA-Alexa 488 and PLGA-FPR 648, were analyzed by flow cytometry and Green (Alexa 488) and Red2 (FPR 648) fluorescence signals were recorded and displayed as dot plots. A quadrant has been set to delineate the different types of particle present in the preparation: upper left, Lpx (lipoplex); lower left, Ls (liposome); lower right, PLGA (PLGA nanoparticles) and Sphs (spherosome); upper right, Sphx (spheroplex). (B) Distribution of the different particle populations in Sphx 2 or Sphx 5 preparations analyzed according to the strategy presented in A (n=7 for Sphx 2 and n=5 for Sphx 5). Note that in a dispersion of Lpx, 4% of Lps is detected.

Non-fluorescent particles are liposomes (Lps), particles with only green fluorescence (Alexa 488) are Lpx (no PLGA), particles with only far red fluorescence (FRP645) (no siRNA) are either PLGA nanoparticles, or spherosomes (PLGA matrix + lipid corona), and particles exhibiting both fluorescence signals are Sphx. We therefore prepared Sphx by adding a solution of PLGA-FRP645 to a dispersion of Lpx prepared with siRNA-Alexa 488 and then analyzed the obtained particles by flow cytometry. We found that nanoparticles dispersion contained 86 ± 10% (n=7) of Sphx for the preparation with 2 µg/µl of PLGA and 77 ± 16% (n=5) of Sphx for the preparation with 5 µg/µl of PLGA (FIG.5B). For both PLGA concentrations conditions, lipoplexes represented only 1% of the particle population, liposomes less than 10%, the remaining particles (10-15%) being PLGA nanoparticles and / or spherosomes. The particle distribution was not significantly different between the two preparation conditions (PLGA 2 or 5 µg/µL). Taken together, these results confirmed that (i) Sphx were the main particles in the dispersion, (ii) siRNAs were effectively associated with Sphx, and (ii) Lpx were sporadically/occasionally detected after nanoprecipitation, upon addition of PLGA.

3.3. Efficacy of Spheroplexes for the delivery of siRNA

3.3.1. In vitro gene silencing efficacy of Sphx on cultured cells

Next, Sphx were prepared with siRNAs specifically targeting luciferase to be tested on cells constitutively expressing luciferase (B16-Luc). We compared their gene silencing efficacy with that of Lpx. As shown in FIG.6A, Sphx were significantly more efficient than Lpx. The gene silencing induced by Lpx or Sphx was specific since no inhibition was observed when control siRNA was used (not shown). Regarding toxicity, regardless of the concentration of PLGA used in the preparation of Sphx, they induced less cytotoxicity than Lpx at equivalent concentrations of siRNA (FIG.6B).
In an effort to explain the difference in gene silencing efficacy between Lpx and Sphx, we examined the evolution in particle efficacy over time, to determine if any of the particle types appeared to be more stable in terms of efficacy. Lpx and Sphx, made with a PLGA solution at 2 µg/µl or 5 µg/µl, were prepared with siRNA-Luc and stored either at controlled room temperature or at 4 °C, and their gene silencing efficacy was assayed 1 day or 1, 2 or 3 week(s) after their preparation. We observed again that Sphx were more efficient than Lpx. In FIG.6C (left panel), it can be seen that both types of particles were very stable at room temperature. Indeed, Sphx 2 had no loss of efficacy over 3 weeks of storage, whereas Sphx 5 and Lpx lost only around 10% from 3 and 2 weeks, respectively. At 4 °C (FIG.6C, right panel), the differences were more pronounced than at room temperature. From 2 weeks, Lpx lost 40% of efficacy, Sphx 5 more than 70% while Sphx 2 lost only 20%. Overall, the transfection efficacy of Sphx 2 seemed to be the most stable over 3 weeks.

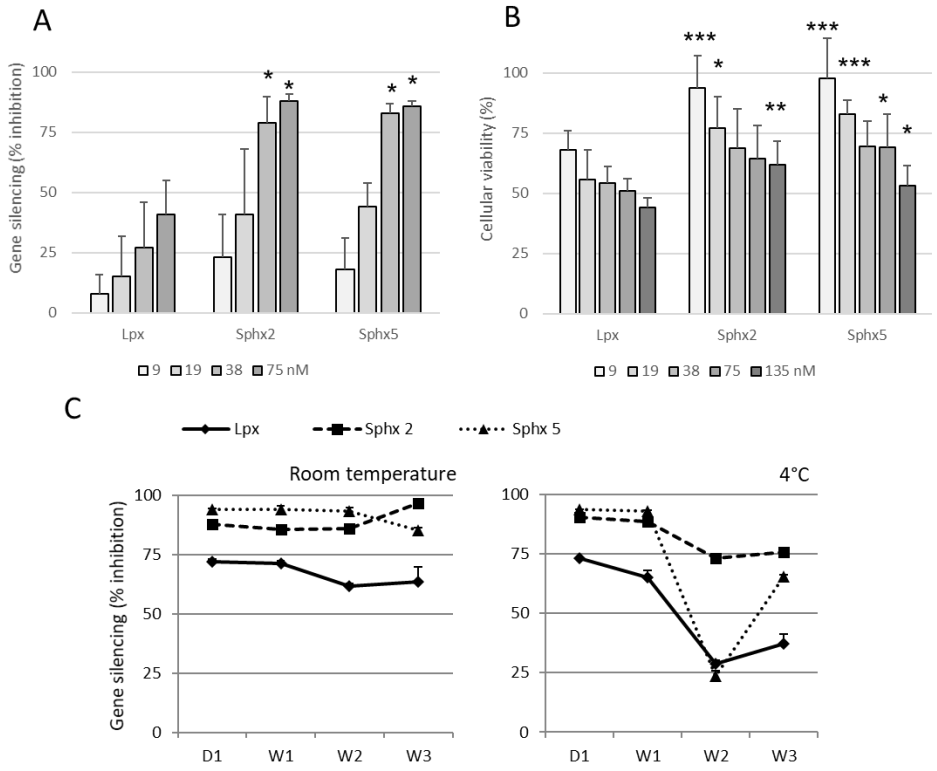

Fig. 6. Assessment of *in vitro* gene silencing efficacy and toxicity of Lpx and Sphx. (A) Lpx and Sphx (2 or 5 µg/µl) were prepared at increasing concentrations of siRNA anti-luciferase and applied on B16-Luc. The results were expressed as % inhibition of luciferase activity relative to non-transfected cells (means ± SD, n=3). (B) Cellular viability of B16-Luc transfected for 24h with Lpx or Sphx prepared at increasing concentrations of siRNA control was evaluated with MTT assay (means ± SD, n=3). (C) Lpx and Sphx were prepared with siRNA anti-luciferase, 3, 2, or 1 week(s) (W3, W2, W1) or the day (D1) before the transfection and stored either at room temperature (left panel) or at 4 °C (right panel) before

being applied on cells. The results were expressed as % inhibition of luciferase activity relative to non-transfected cells. * $p < 0.05$, ** $p < 0.01$, *** $p < 0.005$.

3.3.2. In vivo toxicity

Before evaluating the efficacy of Sphx to orally delivered siRNA, we first performed a toxicity study. We carried out oral administration of Lpx siCtle and Sphx siCtle to mice, then at D+1 and D+7, several parameters were analyzed: the relative weight of the organs (spleen, liver, heart), colon length, expression of inflammatory cytokines (TNF-α, IL-1β, IL-6, MCP-1, INF-γ) in the colon, blood biomarkers (AST, ALT, creatinine) and hematological parameters. The results are presented in Table 2.

Table 2 - Effect of oral administration of Sphx and Lpx in mice.

Mouse treatment	NaCl	Sphx siCtle		Lpx siCtle	
		D1	D7	D1	D7
Relative organ weight (% of mouse weight)					
Spleen	0.44 ± 0.08	0.37 ± 0.07	0.33 ± 0.03 *	0.38 ± 0.06	0.26 ± 0.02 *
Liver	5.56 ± 0.64	5.88 ± 0.75	5.35 ± 0.79	5.73 ± 0.45	5.78 ± 0.32
Heart	0.57 ± 0.01	0.57 ± 0.05	0.60 ± 0.09	0.67 ± 0.10 *	0.70 ± 0.04 *
Colon length (cm)					
	7.48 ± 0.48	7.65 ± 0.46	7.08 ± 0.47	8.35 ± 0.45	7.08 ± 0.40
Cytokines in colon (pg/mg prot)					
TNF-α	10.8 ± 9.3	9.4 ± 3.2	7.5 ± 5.7	16.7 ± 0.7	10.9 ± 4.0
IL-1β	3.9 ± 4.7	0.0 ± 0.0	1.2 ± 1.2	3.2 ± 1.9	2.2 ± 1.7
IL-6	4.5 ± 1.7	6.3 ± 0.8	5.0 ± 1.5	7.9 ± 0.9 *	5.3 ± 1.7
MCP-1	10.1 ± 2.8	15.2 ± 4.8	10.7 ± 4.7	13.2 ± 2.1	11.9 ± 3.0
INF-γ	20.3 ± 12.0	17.6 ± 2.5	14.7 ± 1.1	15.8 ± 2.0	14.1 ± 3.0
Blood biomarkers					
AST (U/L)	359 ± 27	368 ± 121	219 ± 51 *	379 ± 113	394 ± 141
ALT (U/L)	147 ± 44	100 ± 25	120 ± 52	194 ± 76	184 ± 88
Creatinin (µmol/L)	27.0 ± 1.9	25.0 ± 1.7	25.5 ± 1.1	26.3 ± 1.3	26.3 ± 0.8
Hematological parameters					
WBC (10^6 / mL)	6.51 ± 0.81	8.93 ± 1.93	7.16 ± 1.21	5.41 ± 2.89	5.90 ± 0.99
Lymphocytes (% of WBC)	83.3 ± 2.2	80.7 ± 0.6	84.9 ± 1.4	74.0 ± 6.1 *	77.5 ± 1.3 *
Monocytes (% of WBC)	3.5 ± 0.4	4.1 ± 0.4	3.3 ± 0.3	4.5 ± 0.2 *	4.8 ± 0.4 *
Neutrophils (% of WBC)	10.2 ± 2.1	11.8 ± 1.0	8.0 ± 1.1	13.8 ± 4.8	13.2 ± 1.5
Eosinophils (% of WBC)	0.6 ± 0.4	0.4 ± 0.1	1.5 ± 1.0	2.9 ± 1.8	1.7 ± 0.7
Basophils (% of WBC)	1.3 ± 0.1	1.6 ± 0.1 *	1.1 ± 0.2	1.0 ± 0.6	1.4 ± 0.1
Platelets (10^6 / mL)	1061 ± 221	1179 ± 123	1120 ± 144	1203 ± 170	1237 ± 63
RBC (10^9 / mL)	8.48 ± 0.24	8.56 ± 0.06	8.40 ± 0.46	8.07 ± 0.97	8.66 ± 0.28
MCV	45.0 ± 0.8	44.7 ± 0.9	44.2 ± 1.4	44.7 ± 0.7	43.2 ± 0.7 *
Ht (%)	38.2 ± 0.6	38.2 ± 0.7	37.0 ± 1.1	36.0 ± 3.9	37.5 ± 1.8
Hg (g/dL)	13.1 ± 0.5	13.7 ± 0.6	13.0 ± 0.3	12.6 ± 1.8	13.2 ± 0.6

* Represents significant difference from the NaCl group (Mann-Whitney test using two-tailed P-values, $p < 0.05$), Values are mean ± SD, n=4. Abbreviations: AST, aspartate aminotransferase; ALT, alanine aminotransferase; WBC, white blood cells; RBC, red blood cells; Hb, hemoglobin; Ht, hematocrit; MCV, mean corpuscular volume;

A significant increase, compared to control mice (to which only NaCl was given), was detected for the following parameters: (i) the relative weight of the heart for the mice treated with Lpx siCtle, at D+1 and D+7, (ii) the level of IL-6 in the colon for mice treated with Lpx siCtle, at D+1, (iii) the percentage of lymphocytes and monocytes for the mice treated with Lpx siCtle, at D+1 and D+7, (iv) the percentage of basophils for mice treated with Sphx siCtle, on D+1. Other significant difference were decreased. These changes mainly relate to Lpx delivery and are very slight increases. The only increase observed due to treatment with Sphx concerned a very slight increase in the percentage of basophils on D+1 which was no longer detectable on D+7. These data show that oral administration to mice of Sphx particles induced nearly no toxicity, whereas some toxic signs were observed following the administration of Lpx.

3.3.3 In vivo efficacy, DSS-induced ulcerative colitis on mouse

We then evaluated the efficacy of Sphx in delivering siRNA to an organism. Because of their sound stability, we chose to deliver Sphx via oral route in a model of DSS-induced ulcerative colitis in mice. This model of colitis has already been described in the literature [48] to study the efficacy of siRNA delivery systems. The reported consequences for mice of consuming DSS in drinking water are shortening and damage to the colon, as well as local and systemic inflammation.

Male C57bl/6 mice were given water containing 4% DSS for 7 days (FIG.S5A). At D7, mice were sacrificed, blood and colon were collected. Histological sections of the colon were taken to assess specific lesions; cytokine levels were measured in blood or in colon protein extracts. As shown in FIG.S5, mice drinking water supplemented with DSS 4% exhibited a significant decrease in weight (Fig.S5B) and colon length (FIG.S5C) compare to control mice. We also observed a significant increase in the serum level of the chemokine KC (FIG.S5D), as well as in the level of several cytokines in colon protein extracts (FIG.S5E), including TNF-α (FIG.S5F). In addition, intestinal tissue from DSS-drinking mice exhibited clear signs of inflammation including cell infiltration, goblet cell depletion, and irregular mucosal structure (FIG.S5G-J) compared to tissue of control mice.

We also analyzed the expression of inflammatory cytokines (TNF-α, IL-1β, IL-6, MCP-1, INF-γ) in the colon and blood biomarkers (AST, ALT, creatinine), in mice with DSS-induced ulcerative colitis and having received Lpx siCtle or Sphx siCtle treatment every day for 6 days. Analyzes were carried out on D+7. The results are presented in the Table 3.

No significant increase was observed in mice receiving Lpx siCtle or Sphx siCtle compared to mice given only NaCl, neither for cytokines nor for blood markers. However, a significant decrease in the expression of TNF-α and INF-γ was observed in mice treated with Sphx siCtle compared to NaCl mice. This point is discussed in the Discussion part.

Table 3- Effect of oral administration of Sphx and Lpx in mice with DSS-induced colitis.

Mouse treatment	Water	DSS 4%		
		NaCl	Sphx siCtle	Lpx siCtle
Cytokines in colon (pg/mg prot)				
TNF-α	12 ± 6	56 ± 33	26 ± 16 **	73 ± 54
IL-1β	9 ± 10	203 ± 135	228 ± 159	234 ± 210
IL-6	9 ± 3	151 ± 128	235 ± 149	79 ± 21
MCP-1	8 ± 3	180 ± 75	177 ± 48	288 ± 129
INF-γ	33 ± 14	30 ± 10	21 ± 14 *	20 ± 6
Blood biomarkers				
AST (U/L)	262 ± 107	213 ± 36	274 ± 70	227 ± 47
ALT (U/L)	139 ± 31	68 ± 18	98 ± 75	62 ± 8
Creatinin (µmol/L)	28.8 ± 1.9	24.8 ± 1.6	24.6 ± 2.4	26.2 ± 1.5

* Represents significant difference from the NaCl group (Mann-Whitney test using two-tailed P-values, $p < 0.05$), Values are mean ± SD, n= 10 for the water group; n= 12 for the DSS + NaCl group; n= 12 for the DSS + Sphx siCtrl group; and n= 7 for the DSS group + Lpx siCtrl.

As in [49], we chose TNF-α as the target for the delivered siRNA. The gene silencing efficacy of two siRNAs specific for mouse TNF-α were assayed on cells in order to identify the most active sequence (FIG.S6A). Sphx and Lpx were then prepared with the most active siRNA directed against TNF-α (siTNF2) or control siRNA (siCtl), and an *in vitro* transfection was carried out (FIG. S6B), which showed that both types of particles were effective and specific to silence the expression of TNF-α on cells. Then these particles (Sphx 5, the most effective formulation on cells, Lpx, or saline) were administered daily by oral gavage for 6 days to mice under 4% DSS (FIG.7A).

Administration of Sphx siTNF reduced the decrease in colon length (FIG.7B). The difference in colon length between mice treated with Sphx siTNF and that of mice treated with Sphx siCtle or not treated (saline) is significant. Likewise, the mice treated with Sphx siTNF showed a decrease in the level of TNF-α in the colon (FIG.7C) and of KC in serum (FIG.7D). Here again a significant difference was observed with mice treated with Sphx siCtle or untreated mice. In contrast, no effect of Lpx siTNF was observed, either on colon length or on cytokine levels. No significant effect of Sphx siTNF was observed either, on the levels of other cytokines than TNF-α or KC (FIG.S7).

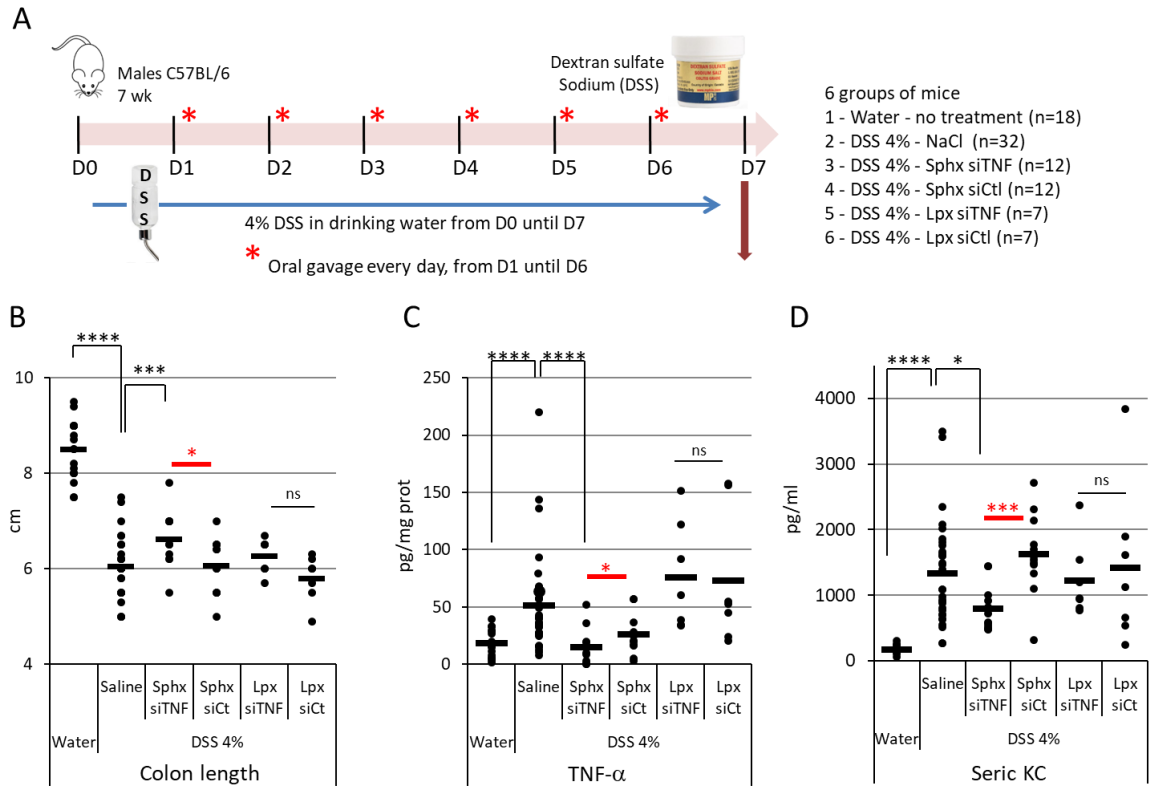

Fig. 7. Assessment of *in vivo* gene silencing efficacy of Sphx and Lpx. (A) Schematic representation of the evaluation of siRNA formulations on a mouse model of DSS-induced ulcerative colitis. The mice under 4% DSS in drinking water were daily orally given, from D1 to D6, Lpx or Sphx 5 prepared with siRNA anti-TNF-α (siTNF2) or siRNA control (siCt) (1 mg siRNA/kg), or saline. On D7, the length of the colon was measured (B), and the level of TNF-α on a colon protein extract (C) and of KC on serum (D) was evaluated by ELISA. * $p < 0.05$, ** $p < 0.01$, *** $p < 0.005$, **** $p < 0.001$; water, n=19; saline, n=32; Lpx (siTNF or siCtle), n= 7; Sphx (siTNF or siCtle), n=12). (B-D), if the number of dots does not appear to match the number of mice, it is because some values were the same for different animals.

3.3.4 Biodistribution study of siRNA among immune cells on DDS-induced colitis mice

A biodistribution study was carried out. Lpx and Sphx prepared with fluorescent Ctle siRNAs (Alexa 647) were administered by gavage to mice with DSS-induced ulcerative colitis. The following day, the mesenteric lymph nodes, the spleen and the colon of the mice were removed. After dissociation of these organs, isolated cells were stained by a cocktail of antibodies allowing to identify by flow cytometry the large immune populations such as T lymphocytes, B lymphocytes and cells of myeloid origin (monocytes, macrophages, DC). The presence of the fluorescent siRNA in these cells was also evaluated by flow cytometry. No siRNA-associated fluorescence was found in immune cells isolated from mesenteric lymph nodes or spleen. The gating strategy presented in FIG.S8 was used on cells dissociated from colonic fragment. Cells were first selected according to their size and granularity and then after excluding cell duplicates, the presence of APC fluorescence (specific to Alexa 647-siRNA fluorescence) was evaluated among the living cells. Both APC positive (having incorporated the fluorescent siRNA) and negative cells were observed among the living cells.

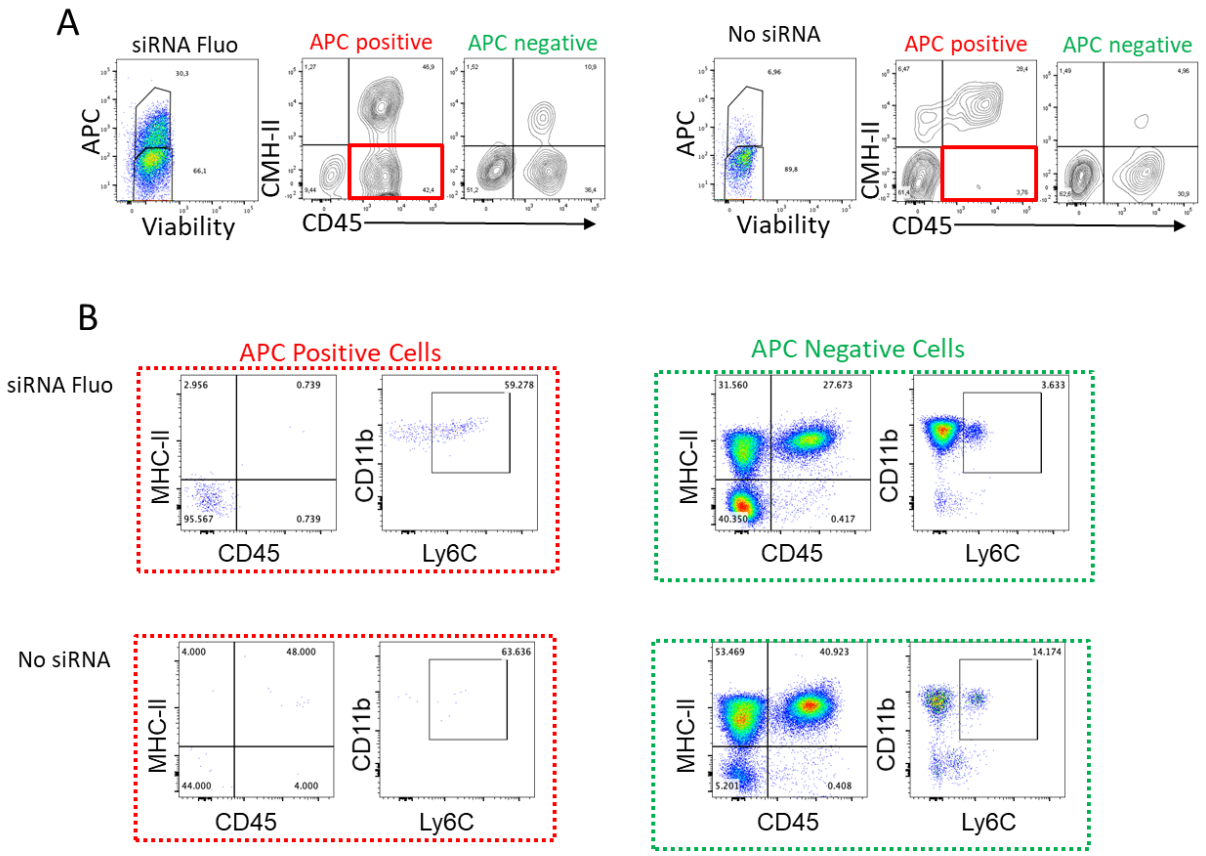

Fig 8. Characterization of immune cells associated with fluorescent siRNA. The mice under 4% DSS in drinking water for 6 days were orally given Lpx or Sphx 5 prepared with fluorescent siRNA control (siRNA fluo, Alexa-647 fluorescence detected in APC channel) or NaCl (no siRNA). Both APC-positive and –negative population were stained specific antibodies (CD45, MHC-II, CD11b and Ly6C). (A) Cells dissociated from colonic fragment, (B) cells from blood. A representative experiment is given as an example.

Among the APC-positive cells, a majority were leukocytes (CD45+) and two populations can be distinguished according to the expression of the MHC-II molecule. CD45+MCH-II+ cells are composed of a low proportion of B lymphocytes (CD19+) and a high percentage of dendritic cells expressing the following phenotype CD11c+CD11b+Ly6c-Ly6g-. CD45+MHC-II- cells, include a low amount of T lymphocytes (CD3+) and a higher percentage of monocytic cells (CD11c-CD11b+Ly6c+Ly6g- phenotypes). In APC-negative cell populations, fewer leukocytes (CD45+) are observed than in APC-positive cells. Among CD45+MHC-II+ cells, the proportions of B cells (CD19+) and dendritic cells (CD11c+CD11b+Ly6c-Ly6g-) are comparable to those found in APC-positive cells. On the other hand, for the CD45+MHC-II- cells, a lower frequency of monocytic cells (CD11c-CD11b+Ly6c+Ly6g- phenotype) was found compared to that found in the APC-positive fraction. The difference in frequency of this monocyte population, observed between APC-positive and APC-negative cells, suggests that these cells may represent a primary target of fluorescent siRNA delivered by Lpx or Sphx in this model.

This result can be confirmed by the analysis presented in FIG.8A. The same staining has been performed in colonic cell suspension from mice fed or not with a fluorescent siRNA. In the absence of the fluorescent siRNA, a weak APC signal representing the fluorescence background of our experiment was observed. By analyzing this APC-positive population in colon samples from mice not fed with fluorescent siRNA, we observed the absence of CD45+CMH-II+ leukocytes that contain the monocytic cell population and that we found in APC-positive cells from mice fed with fluorescent siRNA, demonstrating the specificity of our staining. The percentage of colonic immune cells associated with the fluorescent siRNA was highly variable from one mouse to another, probably because colonic lesions induced by DSS are variable from one individual to another. This variability was also observed for the levels of cytokines measured in the colon of diseased mice (FIG.S5D-F). Moreover, we did not observe any significant difference between the mice having received Lpx or Sphx. The presence of siRNA was also evaluated in blood from treated mice, following a similar gating strategy (FIG.S9). Although the percentage of cells positive for APC was generally lower in blood cells than in cells from the colon, the same staining was found, pointing to the same population of monocytic cells (FIG.8B).

4. Discussion

Polymer lipid hybrid nanoparticles (PLHNP) have been one of the promising non-viral vectors widely investigated in the development of siRNA-based therapeutic delivery systems for *in vivo* administration mostly by parenteral routes of administration [25, 36-38]. In this work, we have shown that siRNA lipoplexes (Lpx) can be easily transformed into PLHNP (Spheroplexes, Sphx) using a simple modified nanoprecipitation method. In the conventional method of nanoprecipitation, surfactants are often added in aqueous and/or organic phases in order to reduce the diameter and aggregation of the nanoparticles [33, 50]. PLGA is one of the most widely used polymers for preparing nanoparticles by this method and different types of end-groups or functionalization are commercially available. When PLGA with carboxylic end groups is used, negatively charged nanoparticles form spontaneously in absence of surfactants [51]. Here, the ester-capped PLGA was chosen to form the polymeric matrix of hybrid nanoparticles, because its end groups are neutral, which prevents any risk of electrostatic interaction with positively charged siRNA Lpx [41]. Under this condition, the excess of lipids from the high +/- charge ratio siRNA Lpx dispersion, used as the aqueous phase, acted as stabilizer and the Sphx dispersion was successfully obtained without the need to add any surfactants. The amphiphilic nature of lipids and their use as surfactant in the preparation of PLHNPS has already been described [52-53]. Here, the stabilizing effect of lipids was confirmed by the fact that spherosomes were obtained with the same modified nanoprecipitation method, replacing Lpx with liposomes (FIG.S1B). The particles obtained exhibit different morphological characteristics, starting from the irregular structures of lipoplexes to give spherical-shaped Sphx, as shown by SEM and AFM in FIG.1. Sphx are positively charged nanoparticles, which have higher mean hydrodynamic diameter and polydispersity index than Lpx (Table 1). Morphological characterization by TEM and cryo-TEM provided additional information on the internal structure of the particles. Lpx, as previously reported [41], are lipid nanoparticles consisting mainly of concentric multi-lamellar structures and a few disordered structures (FIG.2A, 2J). The shape of Sphx is spherical, similar to PLGA nanoparticles, with a large variation of particle size as indicated by the PDI values obtained by the DLS technique. Unlike PLGA nanoparticles, Sphx prepared at both concentrations of PLGA presented a white inner part covered with a typical grey corona which has also been observed

as a uniform dark shell in ultra-thin sections using TEM (FIG.2D-I). Considering the positive ζ potential of Sphx and the ability of osmium tetroxide to stain lipids, TEM images indicate a reorganization of lipids with PLGA in the form of hybrid nanoparticles exhibiting a shell with variable apparent thickness. Unlike TEM, cryo-TEM allowed the observation of Sphx without the interference of sample dehydration and staining. Cryo-TEM images showed that Sphx is a complex heterogeneous dispersion of particles, including Lpx and liposomes. Sphx were identified as grey particles exhibiting thick multilamellar lipid bilayers on the surface, similar to Lpx, and sometimes with the presence of some structures inside nanoparticles seeming small fragments of Lpx or small liposomes. Despite this complexity, cryo-TEM images corresponded to SAXS analysis of nanoparticle structures showing that the Sphx preparation method induced a selective reorganization of lipids in a single lamellar phase. The dispersions of liposomes, Lpx and spherosomes exhibit a mixture of cubic and lamellar phases (FIG.3A and FIG.S3), with phase ratios and q values different from those of Sphx. Even if the supramolecular organization of the lipids in Lpx and Sphx was modified, their atomic composition at the surface of the nanoparticles (≈ 10 nm) was very similar as shown by XPS data (FIG.3B). Additionally, we have demonstrated that the modified nanoprecipitation method preserves the molecular integrity of siRNAs and their association with Sphx. Together with the structural and surface composition data, these results suggest that siRNA molecules are probably not encapsulated in the PLGA inner part, but rather protected between two lipid bilayers, originated from Lpx, and forming the shell of Sphx.

The modified nanoprecipitation method has been used by other research groups for the vectorization of siRNA into PLHNPs. Yang and coll. [35] prepared PLHNPs by single-step nanoprecipitation using cationic lipid (BHEM-Chol) as stabilizer. Hybrid nanoparticles were composed of a core of hydrophobic polylactide acid (PLA), amphiphilic mPEG-PLA forming hydrophilic shell and a monolayer of cationic lipid (BHEM-Chol) at the core-shell interface. Then, in a second step, anionic siRNA molecules were complexed on the surface of the obtained LPHNPs. This hybrid siRNA delivery system presented high physicochemical stability and it was able to inhibit tumor growth in mouse model of BT474 xenograft after intravenous injection. In another study, small hybrid nanoparticles (< 150 nm) with siRNA complexed at the surface (*post*-LPH) or encapsulated into a polymeric core (*in situ*-LPH) were obtained through a single step nanoprecipitation self-assembly method using a high temperature (70 °C) mixture of PLGA, three lipids and Tween 80 as surfactant, followed by an ultrafiltration step for hybrid nanoparticles separation from free siRNA [36]. *In situ*-LPH had a positive surface charge and presented a spherical core-shell morphology formed by polymeric matrix and a lipid-coat. The study of physicochemical stability, tested by incubation in 50% serum up to 24h, showed that *in situ*-LPH were more stable than *post*-LPH, suggesting that siRNA encapsulation offers better protection against siRNA desorption and protein interactions in serum containing medium. Sphx described in this work exhibited similar physicochemical characteristics to the PLHNP reported in previously studies, with a major difference regarding their higher hydrodynamic diameter and PDI. The qualitative and quantitative characterization of nanoparticles populations carried out on Sphx dispersions prepared with fluorescent PLGA-FRP645 and Lpx containing siRNA-Alexa 488 was evaluated thanks to flow cytometry. Using this method, we noticed that Sphx correspond to 77-86% and Lpx less than 1% of the total nanoparticle population. Thus, siRNA molecules were almost completely associated to Sphx (FIG.5). However, Sphx dispersions contained around 20% of other types of nanoparticles, such as PLGA nanoparticles, spherosomes or liposomes. These results were in accordance with high polydispersity of Sphx measured by DLS and the heterogenicity of

nanoparticles with different structures observed by cryo-TEM images (FIG.2K). In order to reduce or eliminate unwanted nanoparticles, the modified nanoprecipitation method presented in this study requires further optimization of certain parameters such as the aqueous/organic phase ratio and more precise control of the mixture. Nanoprecipitation is a simple batch-mode method for the preparation of polymeric and hybrid nanoparticles which had been adapted in recent years to flow-based preparation methods, such as microfluidics systems, to obtain size-controlled and homogeneous nanoparticles dispersion [54-56]. The preparation of small cationic lipid-polymer hybrid nanoparticles dispersion with narrow size distribution for vectorization of siRNA was recently obtained using a specific microfluidic technology named slightly modified swirling microvortex reactor [38, 57]. The adaptation of our method to prepare Sphx using a nanoprecipitation assisted with a microfluidic system will be considered in future studies.

The *in vitro* gene silencing in cells was significantly increased when a specific siRNA (anti-luciferase) was vectorized in Sphx compared to Lpx. Although the literature reports that the size of nanoparticles generally increases with the polymer concentration [58], here we showed that the Sphx size is related to the ratio between polymer concentration and Lpx amount, with PLGA at 5 mg/ml being the concentration which resulted in the smallest nanoparticles (Sphx5). Interestingly, we also showed that Sphx are more stable after storage at controlled room temperature than at 4 °C. When stored at room temperature, Sphx2 maintained gene silencing efficacy over 3 weeks and Sphx5 lost around 10% from 2 and 3 weeks (FIG.6C). This difference is probably due to the fact that the lipids change conformation at low temperature and fail, or in a non-reproducible way, to regain their active conformation when they were incubated at 37 °C during transfection assay on cells. Indeed, it has been shown by Koynova et al, that lipid phase transitions are critical for effective transfection of cells [59]. Furthermore, Sphx were significantly less cytotoxic than Lpx (FIG.6B) in accordance with previous studies comparing siRNA PLHNP and siRNA complexed only with cationic lipid [35]. As reviewed by Lv et al. [17], the presence of free cationic liposomes is associated with the high cytotoxicity of lipoplexes. Thus, we supposed that the interaction of PLGA and Lpx might reduce the quantity of free liposomes in Sphx dispersion and, consequently, decrease cytotoxicity. However, flow cytometry data showed that the concentration of liposomes is between 5-8% of total nanoparticles in Sphx compared to 4% in Lpx dispersion (FIG. 5B). Thus, the reduced cytotoxicity observed for Sphx compared to that of Lpx, could be linked to the fact that Sphx would be taken up by cells and processed in the cell according to a mechanism different from that of Lpx. It is well known that the efficacy of gene silencing of nanoparticles is directly related to their surface properties and to their structural and morphological characteristics, which determine their interaction with cell membranes involved in cellular uptake and endosomal escape. Several studies have shown that cationic nanoparticles with different surface composition exhibit dissimilar interactions with plasma or late endosomal membrane lipids, and different endocytic behavior in live cells [60-62]. Another study using particle-based molecular dynamics simulations, concludes that penetration through lipid bilayer membrane depends on the stiffness and surface hydrophobicity of the nanoparticles [63]. Whereas surface analysis showed that Lpx and Sphx are positively charged and have similar surface composition, we speculate that the increase in gene silencing may be linked to structural and/or morphological change in Sphx. The effect of rigidity of PLGA-lipid hybrid nanoparticles on cellular interaction is presented by Sun and collaborators [64]. In their work, they showed that the interfacial water content inside the hybrid nanoparticles is related to the internal components structure and final rigidity. Core-shell hybrid nanoparticles are similar in shape, size,

composition and surface molecules, but the main difference is in their rigidity. Using molecular dynamics simulation, they showed that less rigid core-shell nanoparticles (with higher internal water content) undergo significant deformation into ellipsoidal shape requiring more energy binding to achieve full internalization. In contrast, rigid hybrid nanoparticles (with low internal water content) are able to move more easily through lipid membranes, which improves their efficiency of cellular uptake. Examination of *in vitro* cellular uptake of fluorescent nanoparticles by confocal microscopy confirms that rigid nanoparticles have higher cellular internalization. In the same study, they also showed that hybrid nanoparticles have better stability than PLGA nanoparticles or liposomes, highlighting the advantage of polymeric core-lipid shell vector. More recently, Shen et al. [65] evaluated the membrane wrapping efficiency of soft or rigid nanoparticles, spherical or non-spherical, using coarse-grained molecular dynamics simulations. Their results corroborate previous work showing that soft spherical nanoparticles deform more easily, have greater total energy barrier and therefore required more time to be wrapped than rigid ones. They also demonstrated that the energy barrier of soft nanoparticles increases with their size, but in the case of rigid nanoparticles this barrier is not affected. Even if we have not measured the stiffness of our nanoparticles, we assume that hydrophobic nature of PLGA improves rigidity and probably reduces internal water content in the Sphx structure. Therefore, if we consider Lpx to be softer nanoparticles than Sphx, these data could explain the increased *in vitro* gene silencing efficacy of Sphx even though their mean hydrodynamic diameter is larger than that of Lpx. However, the interpretation of our results in the light of the presented model simulations must be done with caution because they did not consider the case of positively charged nanoparticles, for which nanoparticle-cell membrane interaction could be different.

Finally, we evaluated whether it was possible to administer Sphx *in vivo* for the delivery of siRNA. Due to their size, we opted for oral administration and chose a model of DSS-induced ulcerative colitis. Indeed, Lamprecht et al. [66] showed that 100 nm particles exhibited better accumulation than 1 or 10 nm particles in the inflamed site in a TNBS model. In addition, a positive surface charge would not be a disadvantage. A study focused on the influence of the surface charge of polymeric nanoparticles on the oral administration of siRNAs showed that the positively charged particles offered better target gene silencing (TNF-α) and possessed a higher anti-inflammatory efficacy against acute ulcerative colitis due to their increased accumulation at the site of the disease [67].
In addition, the absence of induction of inflammatory cytokines upon treatment with Lpx or Sphx (with siCtle) on mice under standard diet, contrary to what we observed after intravenous administration [41] is probably due to the use of oral route for the administration of the particles. In this work we have shown that Sphx are able to induce a regression of the signs of the disease (colon size and serum KC level), as well as significantly decrease the level of TNF-α. Administered following the same protocol, Lpx induces no significant effect. Lpx and Sphx exhibit an equivalent surface charge and it is unlikely that the difference in size observed between them could explain the difference in their *in vivo* efficacy.
We noted an unexpected decrease in the level of TNF-α induced by the treatment with Sphx siCtle. This intriguing effect is to be compared with several publications showing that in the DSS-induced colitis model, the level of TNF-α can be modified by various molecules such as lipids [68], sugars [69] and even particles of PLGA [70]. In particular, Beloqui et al. [70] reported a 50% reduction in the level of the TNF-α after administration of unloaded PLGA nanoparticles. It can therefore be considered that Sphx, due to their composition, induce a slight drop in the level of TNF-α, which is why the

specific effect of siRNA TNF-α can only be deduced by comparison with Sphx siCtle and not the NaCl treatment.

In our study, the nanoparticles are loaded with a siRNA targeting the pro-inflammatory cytokine TNF-α, produced by macrophages/monocytes. The biodistribution study, although preliminary, showed that the administered siRNA was found in a population of monocyte-type immune cells. In the DSS-induced colitis model, Waddell et al. [71] have observed a recruitment of a population of monocytes/macrophages (CD11b+, F4/80+, Ly6Chigh) at the level of the lamina propria of the colon. It is possible that the siRNAs associated with Lpx and Sphx were taken up by monocyte-type cells recruited to the lesion sites, capable of circulating and therefore explaining the detection of these cells in the blood, even at very low doses. These results are also to be compared with our previous publications where we showed that Lpx siRNA injected intravenously in a mice arthritis model, allowed the delivery of siRNA to a population of CD11b+/Ly6Chigh monocytes [72].

Sphx appeared more effective than Lpx. We can hypothesize that Sphx are better internalized by macrophages than Lpx and that the hybrid composition and structural organisation of Sphx provides a benefit during this uptake. In accordance with results presented here, a recently study of our team showed that Lpx are sensitive to simulated intestinal fluid whereas silencing efficacy *in vitro* was dramatically decreased after one-hour exposure. In this environment condition, the presence of bile salts probably induce the destabilization of lipoplex structure and exposure of siRNA to nucleases [73]. The *in vivo* data observed with Sphx indicates that our PLHNP might be a promising formulation in the oral administration of siRNA.

Conclusion

The benefit of the association of lipid and polymer in hybrid nanoparticles has been largely studied in order to improve efficacy and safety in drugs and nucleic acid delivery or even as a promising co-delivery system of both molecules [25, 74]. Our promising results open a road of possibilities to improve the production of spheroplexes and their *in vivo* administration. The nanoparticle preparation using microfluidic-based nanoprecipitation technique and the possibility to formulate spheroplexes in tablet forms, as already done for siRNA lipoplexes by our group [75], are some of the perspectives to be explored in near future studies.

Funding
This work was supported by CNPq, CAPES-COFECUB [Ph-C 860-15], FAPEMIG, CNRS, INSERM and Université de Paris.

Declaration of competing interest
None

Acknowledgments
We acknowledge SOLEIL for provision of synchrotron radiation facilities and we would like to thank Javier PEREZ and Youssef LIATIMI for assistance in using beamline SWING. We are also grateful to ESRF (Grenoble, France) and the members of beamline ID02, especially Theyencheri NARAYANAN, for giving us access to the beamline, which allowed us to carry out the preliminary experiments

necessary to develop the following tests. We are grateful to the Animal Platform (in vivo experiments), Unite Mixte de Service (UMS) 3612, CNRS, INSERM US 025, Université de Paris, France. We are also grateful to Nicolas Sorhaindo, Plateforme de Biochimie, CRI, Faculté de Médecine Site Bichat, Paris.

References

[1] A. Fire, S. Xu, M.K. Montgomery, S.A. Kostas, S.E. Driver, C.C. Mello, Potent and specific genetic interference by double-stranded RNA in Caenorhabditis elegans, Nature 391 (1998) 806–811. DOI: 10.1038/35888

[2] S.M. Elbashir, J. Harborth, W. Lendeckel, A. Yalcin, K. Weber, T. Tuschl, Duplexes of 21-nucleotide RNAs mediate RNA interference in cultured mammalian cells, Nature 411 (2001) 494–498. DOI: 10.1038/35078107

[3] D. Adams, A. Gonzalez-Duarte, W.D. O'Riordan, C.C. Yang, M. Ueda, A.V. Kristen, I. Tournev, H.H. Schmidt, T. Coelho, J.L. Berk, K.P. Lin, G. Vita, S. Attarian, V. Planté-Bordeneuve, M.M. Mezei, J.M. Campistol, J. Buades, T.H. Brannagan, B.J. Kim, J. Oh, Y. Parman, Y. Sekijima, P. Hawkins, S.D. Solomon, M. Polydefkis, P.J. Dyck, P.J. Gandhi, S. Goyal, J. Chen, A.L. Strahs, S.V. Nochur, M.T. Sweetser, P.P. Garg, A.K. Vaishnaw, J.A. Gollob, O.B. Suhr, Patisiran, an RNAi Therapeutic, for Hereditary Transthyretin Amyloidosis, N. Engl. J. Med. 379 (2018) 11–21. DOI: 10.1056/NEJMoa1716153

[4] Y. Weng, H. Xiao, J. Zhang, X.-J. Liang, Y. Huang, RNAi therapeutic and its innovative biotechnological evolution, Biotechnol. Adv. 37 (2019) 801–825. DOI: 10.1016/j.biotechadv.2019.04.012

[5] S. Agarwal, A.R. Simon, V. Goel, B.A. Habtemariam, V.A. Clausen, J.B. Kim, G.J. Robbie, Pharmacokinetics and Pharmacodynamics of the Small Interfering Ribonucleic Acid, Givosiran, in Patients With Acute Hepatic Porphyria. Clin. Pharmacol. Ther. 108 (2020) 63-72. DOI: 10.1002/cpt.1802

[6] L.J. Scott, S.J. Keam, Lumasiran: First Approval. Drugs 81 (2021) 277–282. DOI: 10.1007/s40265-020-01463-0

[7] M. Caillaud, M. El Madani, L. Massaad-Massade, Small interfering RNA from the lab discovery to patients' recovery, J. Control. Release 321 (2020) 616–628. DOI: 10.1016/j.jconrel.2020.02.032

[8] M.A. Subhan, V.P. Torchilin, siRNA based drug design, quality, delivery and clinical translation, Nanomedicine (2020) 102239. DOI: 10.1016/j.nano.2020.102239

[9] V. Busignies, C. Charrueau, P. Tchoreloff, V. Escriou, Nanostructures for oral delivery of therapeutic nucleic acids, in: E. Andronescu, A. Mihai (Eds.), Nanostructures for Oral Medicine, Elsevier, New York, (2017) 147–172. ISBN 978-0-323-47720-8. (2017) 147–169.

[10] Z. Meng, M. Lu, RNA Interference-Induced Innate Immunity, Off-Target Effect, or Immune Adjuvant? Front. Immunol. 8 (2017) 331. DOI: 10.3389/fimmu.2017.00331

[11] M.I. Sajid, M. Moazzam, S. Kato, K. Yeseom Cho, R.K. Tiwari, Overcoming Barriers for siRNA Therapeutics: From Bench to Bedside, Pharmaceuticals (Basel). 13 (2020) 294. DOI: 10.3390/ph13100294

[12] B. Kim, J.H. Park, M.J. Sailor, Rekindling RNAi Therapy: Materials Design Requirements for In Vivo siRNA Delivery, Adv. Mater. 49 (2019) e1903637. DOI: 10.1002/adma.201903637

[13] S. Yonezawa, H. Koide, T. Asai, Recent advances in siRNA delivery mediated by lipid-based nanoparticles, Adv Drug Deliv Rev. 154-155 (2020) 64-78. DOI: 10.1016/j.addr.2020.07.022

[14]N. Dan, D. Danino, Structure and kinetics of lipid-nucleic acid complexes, Adv. Colloid. Interface Sci. 205 (2014) 230-239. DOI: 10.1016/j.cis.2014.01.013
[15]S. Akhtar, I. Benter, Toxicogenomics of non-viral drug delivery systems for RNAi: potential impact on siRNA-mediated gene silencing activity and specificity, Adv. Drug Deliv. Rev. 59 (2007) 164-182. DOI: 10.1016/j.addr.2007.03.010
[16]P. Vader, L. J. van der Aa, G. Storm, R.M. Schiffelers, J.F. Engbersen, Polymeric carrier systems for siRNA delivery, Curr. Top. Med. Chem. 12 (2012) 108-119. DOI: 10.2174/156802612798919123
[17]H. Lv, S. Zhang, B. Wang, S. Cui, J. Yan, Toxicity of cationic lipids and cationic polymers in gene delivery, J. Control. Release 114 (2006) 100-109. DOI: 10.1016/j.jconrel.2006.04.014
[18]S. Jesus, M. Schmutz, C. Som, G. Borchard, P. Wick, O. Borges, Hazard Assessment of Polymeric Nanobiomaterials for Drug Delivery: What Can We Learn From Literature So Far, Front Bioeng. Biotechnol. 7 (2019) 261. DOI: 10.3389/fbioe.2019.00261
[19]R. Rai, S. Alwani, I. Badea, Polymeric Nanoparticles in Gene Therapy: New Avenues of Design and Optimization for Delivery Applications, Polymers (Basel) 11 (2019) 745. DOI: 10.3390/polym11040745
[20]F. Molavi, M. Barzegar-Jalali, H. Hamishehkar, Polyester based polymeric nano and microparticles for pharmaceutical purposes: A review on formulation approaches, J. Control. Release 320 (2020) 265-282. DOI: 10.1016/j.jconrel.2020.01.028
[21]A. Mohanty, S. Uthaman, I.-K. Park, Utilization of Polymer-Lipid Hybrid Nanoparticles for Targeted Anti-Cancer Therapy, Molecules 25 (2020) 4377. DOI: 10.3390/molecules25194377
[22]J.M. Chan, L. Zhang, K.P. Yuet, G. Liao, J.W. Rhee, R. Langer, O.C. Farokhzad, PLGA-lecithin-PEG core-shell nanoparticles for controlled drug delivery, Biomaterials 8 (2009) 1627-1634. DOI: 10.1016/j.biomaterials.2008.12.013
[23]W. Hasan, K. Chu, A. Gullapalli, S.S. Dunn, E.M. Enlow, J.C. Luft, S. Tian, M.E. Napier, P.D. Pohlhaus, J.P. Rolland, J.M. DeSimone, Delivery of multiple siRNAs using lipid-coated PLGA nanoparticles for treatment of prostate cancer, Nano Lett. 12 (2012) 287-292. DOI: 10.1021/nl2035354
[24]A.J. Mieszawska, Y. Kim, A. Gianella, I. van Rooy, B. Priem, M.P. Labarre, C. Ozcan, D.P. Cormode, A. Petrov, R. Langer, O.C. Farokhzad, Z.A. Fayad, W.J. Mulder, Synthesis of polymer-lipid nanoparticles for image-guided delivery of dual modality therapy, Bioconjug. Chem. 24 (2013) 1429-1434. DOI: 10.1021/bc400166j
[25]X. Zhao, F. Li, Y. Li, H. Wang, H. Ren, J. Chen, G. Nie, J. Hao, Co-delivery of HIF1alpha siRNA and gemcitabine via biocompatible lipid-polymer hybrid nanoparticles for effective treatment of pancreatic cancer, Biomaterials 46 (2015) 13-25. DOI: 10.1016/j.biomaterials.2014.12.028
[26]M.A.A. Jansen, L.H. Klausen, K. Thanki, J. Lyngsø, J. Skov Pedersen, H. Franzyk, H.M. Nielsen, W. van Eden, M. Dong, F. Broere, C. Foged, X. Zeng, Lipidoid-polymer hybrid nanoparticles loaded with TNF siRNA suppress inflammation after intra-articular administration in a murine experimental arthritis model, Eur. J. Pharm. Biopharm. 142 (2019) 38-48. DOI: 10.1016/j.ejpb.2019.06.009
[27]M. Rahman, K.S. Alharbi, N.K. Alruwaili, N. Anfinan, W.H. Almalki, I. Padhy, U. Sambamoorthy, S. Swain, S. Beg, Nucleic acid-loaded lipid-polymer nanohybrids as novel nanotherapeutics in anticancer therapy, Expert Opin. Drug Deliv. 17 (2020) 805-816. DOI: 10.1080/17425247.2020.1757645

[28]S. Rao, C.A. Prestidge, Polymer-lipid hybrid systems: merging the benefits of polymeric and lipid-based nanocarriers to improve oral drug delivery, Expert Opin. Drug Deliv. 13 (2016) 691–707. DOI: 10.1517/17425247.2016.1151872

[29]K. Thanki, D. van Eetvelde, A. Geyer, J. Fraire, R. Hendrix, H. Van Eygen, E. Putteman, H. Sami, C. de Souza Carvalho-Wodarz, H. Franzyk, H.M. Nielsen, K. Braeckmans, C.M. Lehr, M. Ogris, C. Foged, Mechanistic profiling of the release kinetics of siRNA from lipidoid-polymer hybrid nanoparticles in vitro and in vivo after pulmonary administration, J. Control. Release 310 (2019) 82-93. DOI: 10.1016/j.jconrel.2019.08.004

[30]Y. Xu, A. Thakur, Y. Zhang, C. Foged, Inhaled RNA Therapeutics for Obstructive Airway Diseases: Recent Advances and Future Prospects, Pharmaceutics. 13 (2021) 177. DOI: 10.3390/pharmaceutics13020177

[31]S. Maghrebi, C.A. Prestidge, P. Joyce, An update on polymer-lipid hybrid systems for improving oral drug delivery, Expert Opin. Drug Deliv. 16 (2019) 507-524. DOI: 10.1080/17425247.2019.1605353

[32]R. Chevalier, siRNA Targeting and Treatment of Gastrointestinal Diseases, Clin. Transl. Sci. 12 (2019) 573-585. DOI: 10.1111/cts.12668 .

[33]C.J. Martínez Rivas, M. Tarhini, W. Badri, K. Miladi, H. Greige-Gerges, Q.A. Nazari, S.A. Galindo Rodríguez, R. Á. Román, H. Fessi, A. Elaissari, Nanoprecipitation process: From encapsulation to drug delivery, Int. J. Pharm. 532 (2017) 66-81. DOI: 10.1016/j.ijpharm.2017.08.064

[34]H.A. Almoustafa, M.A. Alshawsh, Z. Chik, Technical aspects of preparing PEG-PLGA nanoparticles as carrier for chemotherapeutic agents by nanoprecipitation method, Int. J. Pharm. 533 (2017) 275-284. DOI: 10.1016/j.ijpharm.2017.09.054

[35]X.Z. Yang, S. Dou, Y.C. Wang, H.Y. Long, M.H. Xiong, C.Q. Mao, Y.D. Yao, J. Wang, Single-step assembly of cationic lipid-polymer hybrid nanoparticles for systemic delivery of siRNA, ACS Nano 6 (2012) 4955-4965. DOI: 10.1021/nn300500u

[36]H.M. Abdel-Bar, A.A. Walters, J.T. Wang, K.T. Al-Jamal, Combinatory Delivery of Etoposide and siCD47 in a Lipid Polymer Hybrid Delays Lung Tumor Growth in an Experimental Melanoma Lung Metastatic Model**,** Adv. Healthc. Mater. 10 (2021) e2001853. DOI: 10.1002/adhm.202001853

[37]Y. Liu, T. Long, N. Zhang, B. Qiao, Q. Yang, Y. Luo, J. Cao, J. Luo, D. Yuan, Y. Sun, Y. Li, Z. Yang, Z.G. Wang, Ultrasound-Mediated Long-Circulating Nanopolymer Delivery of Therapeutic siRNA and Antisense MicroRNAs Leads to Enhanced Paclitaxel Sensitivity in Epithelial Ovarian Cancer Chemotherapy, ACS Biomater. Sci. Eng. 6 (2020) 4036-4050. DOI: 10.1021/acsbiomaterials.0c00330

[38]Y. Guo, H. Lee, Z. Fang, A. Velalopoulou, J. Kim, M.B. Thomas, J. Liu, R.G. Abramowitz, Y. Kim, A.F. Coskun, D.P. Krummel, S. Sengupta, T.J. MacDonald, C. Arvanitis, Single-cell analysis reveals effective siRNA delivery in brain tumors with microbubble-enhanced ultrasound and cationic nanoparticles, Sci. Adv. 7 (2021) eabf7390. DOI: 10.1126/sciadv.abf7390

[39]G. Byk, D. Scherman, B. Schwartz, C. Dubertret, Lipopolyamines as Transfection Agents and Pharmaceutical Uses Thereof, US Patent 6171612 (2001).

[40]A. Schlegel, C. Largeau, P. Bigey, M. Bessodes, K. Lebozec, D. Scherman, V. Escriou, Anionic polymers for decreased toxicity and enhanced in vivo delivery of siRNA complexed with cationic liposomes, J. Control. Release 152 (2011) 393–401. DOI: 10.1016/j.jconrel.2011.03.031

[41]D.C. Arruda, I.J. Gonzalez, S. Finet, L. Cordova, V. Trichet, G.F. Andrade, C. Hoffmann, P. Bigey, W.A. de Almeida Macedo, A. Da Silva Cunha Jr, A. Malachias de Souza, V. Escriou, Modifying internal organization and surface morphology of siRNA lipoplexes by sodium alginate addition for

efficient siRNA delivery, J. Colloid Interface Sci. 540 (2019) 342−353. DOI: 10.1016/j.jcis.2019.01.043

[42]A. Schlegel, P. Bigey, H. Dhotel, D. Scherman, V. Escriou, Reduced in vitro and in vivo toxicity of siRNA-lipoplexes with addition of polyglutamate, J. Control. Release 165 (2013) 1-8. DOI: 10.1016/j.jconrel.2012.10.018

[43]M. Agassandian, R.K. Mallampalli, Surfactant phospholipid metabolism, Biochim. Biophys. Acta 1831 (2013) 612-625. DOI: 10.1016/j.bbalip.2012.09.010

[44]V. Escriou, P. Bigey, D. Scherman, Vectors including an anionic macromolecule and a cationic lipid for delivering small nucleic acids, European Patent EP 2389158 (2009) B1.

[45] A. Göpferich, Mechanisms of polymer degradation and erosion, Biomaterials. 17 (1996) 103-114. DOI: 10.1016/0142-9612(96)85755-3

[46] W. Badri, K. Miladi, Q.A. Nazar, H. Fessia, A. Elaissari, Effect of process and formulation parameters on polycaprolactone nanoparticles prepared by solvent displacement, Colloids Surfaces A: Physicochem. Eng. Aspects 516 (2017) 238–244. DOI: 10.1016/j.colsurfa.2016.12.029

[47]A.-L. Troutier, T. Delair, C. Pichot, C. Ladavière, Physicochemical and Interfacial Investigation of Lipid/Polymer Particle Assemblies, Langmuir 21 (2005) 1305-1313. DOI: 10.1021/la047659t

[48]J. Zhang, C. Tang, C. Yin, Galactosylated trimethyl chitosan-cysteine nanoparticles loaded with Map4k4 siRNA for targeting activated macrophages, Biomaterials 34 (2013) 3667-3677. DOI: 10.1016/j.biomaterials.2013.01.079

[49]C. Kriegel, M. Amiji, Oral TNF-α gene silencing using a polymeric microsphere-based delivery system for the treatment of inflammatory bowel disease, J. Control. Release 150 (2011) 77–86. DOI: 10.1016/j.jconrel.2010.10.002

[50]H. Fessi, F. Puisieux, J.P. Devissaguet, N. Ammoury, S. Benita, Nanocapsule formation by interfacial polymer deposition following solvent displacement, Int. J. Pharm. 55 (1989) R1–R4. DOI: 10.1016/0378-5173(89)90281-0

[51]R. Cornu, N. Rougier, Y. Pellequer, A. Lamprecht, P. Hamon, R. Li, A. Beduneau, H. Martin, Interspecies differences in the cytochrome P450 activity of hepatocytes exposed to PLGA and silica nanoparticles: an in vitro and in vivo investigation, Nanoscale 10 (2018) 5171-5181. DOI: 10.1039/c8nr00226f

[52]L. Zhang, J.M. Chan, F.X. Gu, J.W. Rhee, A.Z. Wang, A.F. Radovic-Moreno, F. Alexis, R. Langer, O.C. Farokhzad, Self-assembled lipid-polymer hybrid nanoparticles: a robust drug delivery platform, ACS Nano 2 (2008) 1696-702. DOI: 10.1021/nn800275r

[53]S. Golan-Paz, H. Frizzell, K.A. Woodrow, Cross-Platform Comparison of Therapeutic Delivery from Multilamellar Lipid-Coated Polymer Nanoparticles, Macromol. Biosci. 19 (2019) e1800362. DOI: 10.1002/mabi.201800362

[54]J.W. Hickey, J.L. Santos, J.M. Williford, H.Q. Mao, Control of polymeric nanoparticle size to improve therapeutic delivery, J. Control. Release 219 (2015) 536-547. DOI: 10.1016/j.jconrel.2015.10.006

[55]I. Ottonelli, J.T. Duskey, A. Rinaldi, M.V. Grazioli, I. Parmeggiani, M.A. Vandelli, L.Z. Wang, R.K. Prud'homme, G. Tosi, B. Ruozi, Microfluidic Technology for the Production of Hybrid Nanomedicines, Pharmaceutics 13 (2021) 1495. DOI: 10.3390/pharmaceutics13091495

[56]R. Zoqlam, C.J. Morris, M. Akbar, A.M. Alkilany, S.I. Hamdallah, P. Belton, S. Qi, Evaluation of the Benefits of Microfluidic-Assisted Preparation of Polymeric Nanoparticles for DNA Delivery, Mater. Sci. Eng. C 127 (2021) 112243. DOI: 10.1016/j.msec.2021.112243

[57]R.A. Meyer, G.P. Hussmann, N.C. Peterson, J.L. Santos, A.D. Tuesca, A scalable and robust cationic lipid/polymer hybrid nanoparticle platform for mRNA delivery, Int. J. Pharm. 611 (2022) 121314. DOI: 10.1016/j.ijpharm.2021.121314

[58]E. Lepeltier, C. Bourgaux, P. Couvreur, Nanoprecipitation and the "Ouzo effect": Application to drug delivery devices, Adv. Drug Deliv. Rev. 71 (2014) 86-97. DOI: 10.1016/j.addr.2013.12.009

[59]R. Koynova, L. Wang, R.C. MacDonald, Synergy in Lipofection by Cationic Lipid Mixtures: Superior Activity at the Gel-Liquid Crystalline Phase Transition, J. Phys. Chem. B 111 (2007) 7786-7795. DOI : 10.1021/jp071286y

[60]S. Zhang, H. Gao, G. Bao, Physical Principles of Nanoparticle Cellular Endocytosis, ACS Nano 9 (2015) 8655-8671. DOI: 10.1021/acsnano.5b03184

[61]E. Blanco, H. Shen, M. Ferrari, Principles of nanoparticle design for overcoming biological barriers to drug delivery, Nat. Biotechnol. 33 (2015) 941-951. DOI: 10.1038/nbt.3330

[62]C. Peetla, S. Jin, J. Weimer, A. Elegbede, V. Labhasetwar, Biomechanics and thermodynamics of nanoparticle interactions with plasma and endosomal membrane lipids in cellular uptake and endosomal escape**,** Langmuir 30 (2014) 7522-7532. DOI: 10.1021/la5015219

[63]S. Wang, H. Guo, Y. Li, X. Li, Penetration of nanoparticles across a lipid bilayer: effects of particle stiffness and surface hydrophobicity, Nanoscale 11 (2019) 4025-4034. DOI: 10.1039/c8nr09381d

[64]J. Sun, L. Zhang, J. Wang, Q. Feng, D. Liu, Q. Yin, D. Xu, Y. Wei, B. Ding, X. Shi, X. Jiang, Tunable rigidity of (polymeric core)-(lipid shell) nanoparticles for regulated cellular uptake**,** Adv. Mater. 27 (2015) 1402-1407. DOI: 10.1002/adma.201404788

[65]Z. Shen, H. Ye, X. Yi, Y. Li, Membrane Wrapping Efficiency of Elastic Nanoparticles during Endocytosis: Size and Shape Matter, ACS Nano 13 (2019) 215-228. DOI: 10.1021/acsnano.8b05340

[66]A. Lamprecht, U. Schäfer, C.M. Lehr, Size-dependent bioadhesion of micro- and nanoparticulate carriers to the inflamed colonic mucosa, Pharm. Res. 18 (2001) 788-793. DOI: 10.1023/a:1011032328064

[67]S. Iqbal, X. Du, J. Wang, H. Li, Y. Yuan, J. Wang, Surface charge tunable nanoparticles for TNF-α siRNA oral delivery for treating ulcerative colitis, Nano Res. 11 (2018) 2872–2884. DOI: 10.1007/s12274-017-1918-3

[68]I. Treede, A. Braun, P. Jeliaskova, T. Giese, J. Füllekrug, G. Griffiths, W. Stremmel, R. Ehehalt, TNF-α-induced up-regulation of pro-inflammatory cytokines is reduced by phosphatidylcholine in intestinal epithelial cells, BMC Gastroenterol. 9 (2009) 53. DOI :10.1186/1471-230X-9-53

[69]M. Liao, Y. Zhang, Y. Qiu,Z. Wu, Z. Zhong, X. Zeng, Y. Zeng, L. Xiong, Y. Wen, R. Liu, Fructooligosaccharide supplementation alleviated the pathological immune response and prevented the impairment of intestinal barrier in DSS induced acute colitis mice, Food Funct. 12 (2021) 9844. DOI: 10.1039/d1fo01147b

[70]A. Beloqui, R. Coco, P.B. Memvanga, B. Ucakar, A. des Rieux, V. Préat, pH-sensitive nanoparticles for colonic delivery of curcumin in inflammatory bowel disease, Int. J. Pharm 473 (2014) 203–212. DOI: 10.1016/j.ijpharm.2014.07.009

[71]A. Waddell, R. Ahrens, K. Steinbrecher, B. Donovan, M.E. Rothenberg, A. Munitz, S.P. Hogan, Colonic Eosinophilic Inflammation in Experimental Colitis Is Mediated by Ly6Chigh CCR2+ inflammatory Monocyte/Macrophage-Derived CCL11, J. Immunol. 186 (2011) 5993–6003. DOI: 10.4049/jimmunol.1003844

[72]M. Ammari , J. Presumey , C. Ponsolles, G. Roussignol , C. Roubert , V. Escriou , K. Toupet , A.-L. Mausset-Bonnefont , M. Cren, M. Robin, P. Georgel, R. Nehmar , L. Taams, J. Grün , A. Grützkau , T. Häupl , Y.-M. Pers, C. Jorgensen, I. Duroux-Richard, G. Courties, F. Apparailly, Delivery of miR-146a to Ly6C high Monocytes Inhibits Pathogenic Bone Erosion in Inflammatory Arthritis, Theranostics 8 (2018) 5972-5985. DOI: 10.7150/thno.29313.

[73]A.U. Rehman, V. Busignies, M. Coelho Silva Ribeiro, N. Almeida Lage, P. Tchoreloff, V. Escriou, C. Charrueau, Fate of Tableted Freeze-Dried siRNA Lipoplexes in Gastrointestinal Environment, Pharmaceutics 13 (2021) 1807. DOI: 10.3390/pharmaceutics13111807

[74]M. Zhiani, M.A. Mousavi, K. Rostamizadeh, R. Pirizadeh, A. Osali, A, Mennati, B. Motlagh, M. Fathi, Apoptosis induction by siRNA targeting integrin-β1 and regorafenib/DDAB-mPEG-PCL hybrid nanoparticles in regorafenib-resistant colon cancer cells, Am. J. Cancer Res. 11 (2021) 1170-1184.

[75]V. Busignies, D.C. Arruda, C, Charrueau, M.C.S. Ribeiro, A.-M. Lachagès, A. Malachias, S. Finet A.U. Rehman, P. Bigey, P, Tchoreloff, V. Escriou, Compression of Vectors for Small Interfering RNAs Delivery: Toward Oral Administration of siRNA Lipoplexes in Tablet Forms, Mol Pharm. 17 (2020) 1159-1169. DOI: 10.1021/acs.molpharmaceut.9b01190

Supplementary data

Spheroplexes: hybrid PLGA-cationic lipid nanoparticles, for in vitro and oral delivery of siRNA

Danielle Campiol Arruda, Anne-Marie Lachagès, Hélène Demory, Guillaume Escriou, René Lai-Kuen, Pierre-Yves Dugas, Céline Hoffmann, Stéphanie Bessoles, Guillaume Sarrabayrouse, Angelo Malachias, Stéphanie Finet, Pedro Lana Gastelois, Waldemar Augusto de Almeida Macedo, Armando da Silva Cunha Jr, Pascal Bigey, Virginie Escriou

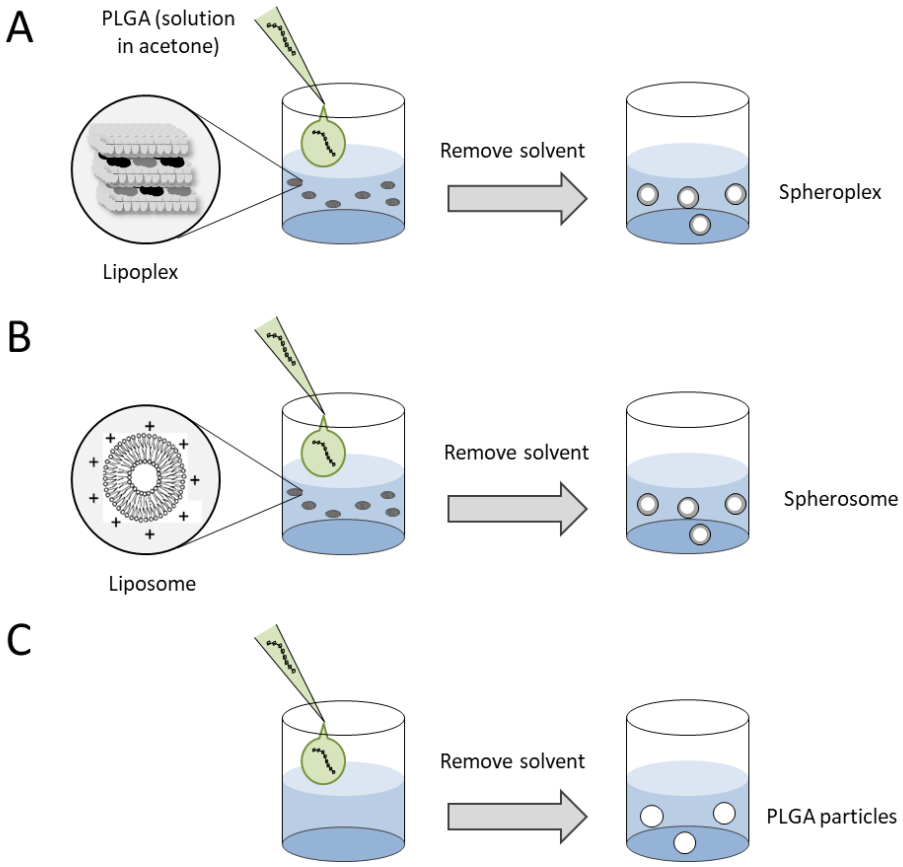

Figure S1 - Preparation of the different types of particles. (A) Spheroplexes are prepared by adding a solution of PLGA in acetone into a dispersion of lipoplexes in a saline buffer and elimination of the solvent (acetone). (B) Spherosomes are prepared according to the same protocol by replacing lipoplexes with liposomes. (C) Injecting the PLGA solution into the saline solution (without dispersion of particles) and removing acetone produces a small amount of PLGA particles.

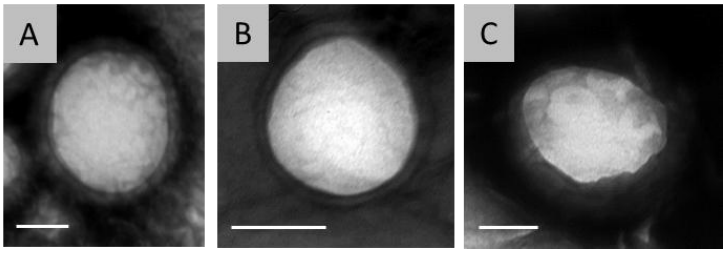

Figure S2 - TEM micrographs of Sphx 5 (A), Sphx 2 (B) and particles obtained by addition of a solution of PLGA to a dispersion of cationic liposome, or spherosomes (C), after negative staining with uranyl acetate. The scale bar is fixed to 100 nm.

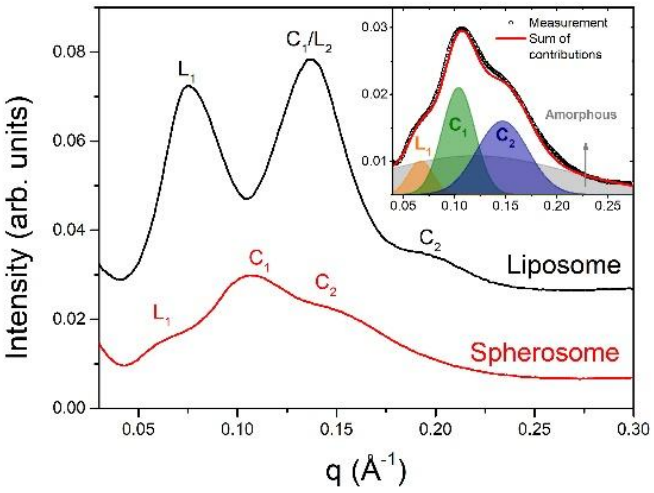

Figure S3 - SAXS profiles of particles in dispersion in 150 mM NaCl. Liposome (black curve) and Spherosome (red curve). Inset, fitting of the spherosome curve, depicting peak components that form the structural signal retrieved for the spherosome dispersion.

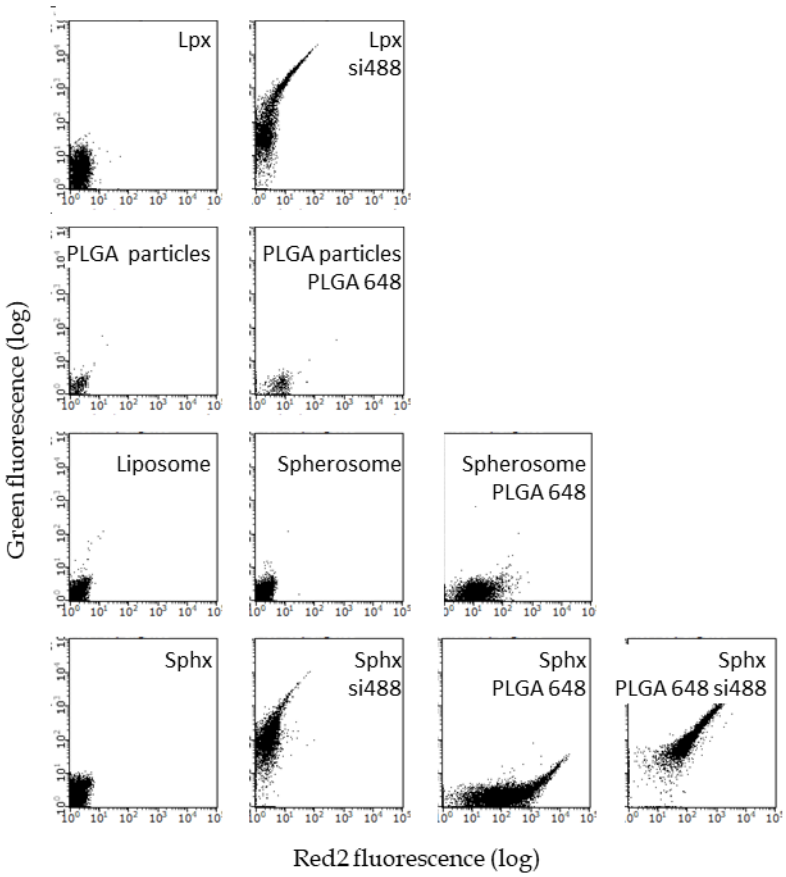

Figure S4 - Representative dot plots from flow cytometry analysis of various particles. Lipoplexes (Lpx), liposomes, spherosomes, spheroplexes (Sphx) or PLGA particles, unlabeled or labeled via incorporation of PLGA-FPR 648 and/or siRNA-A488, were analyzed by flow cytometry and Green (Alexa 488) and Red2 (FPR 648) fluorescence signals were recorded and displayed as dot plots.

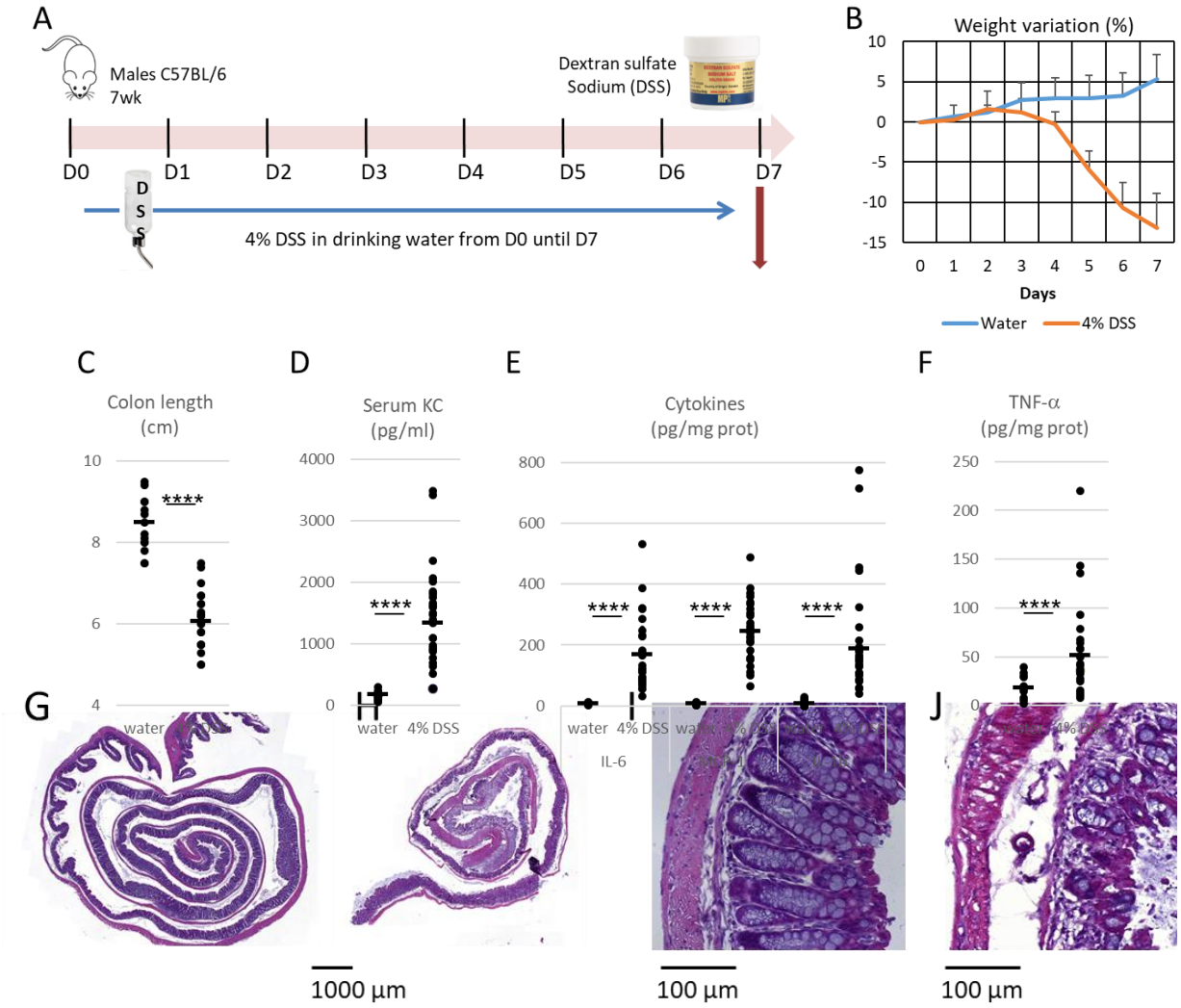

Figure S5 - Mouse DSS-induced colitis model. (A) Schematic representation of the induction of ulcerative colitis in mice. (B) Daily weight variation of mice given 4% DSS in drinking water (4% DSS) compared to untreated mice (water). On D7, the length of the colon was measured (C), and the level of several cytokines, TNF-α (F), IL-6, MCP-1 and IL-1β (E) on a colon protein extract was evaluated by ELISA. The level of KC was also assayed by ELISA on serum (D). **** $p < 0.001$. Colon length, cytokines: water, n=16; 4% DSS, n=32. Weight variation: water, n=15; 4% DSS, n=23. (H, J) Hematoxylin and eosin (H&E) staining of swiss-rolls of the colons of mice given 4% DSS in drinking water compared to unchallenged mice (G, I). (G-H) overview of the complete colon (bar of 1000 µm), (I-J) magnification of an area (bar of 100 µm). Tissue samples corresponded to medial and distal regions of the colon were slit open longitudinally and the contents carefully removed. Next, each segment was rolled up longitudinally, with the mucosa outwards. Finally, the preparation stored overnight in 4% PFA at 4 °C before embedding in paraffin. Cross sections (4µm thick) were stained with haematoxylin and eosin and imaging using Perkin Elmer Lamina scanner (Cochin HistIM Facility). Tissue samples were evaluated for mucosal architectural change, cellular infiltration, inflammation, goblet cell depletion, surface epithelial cell hyperplasia, and signs of epithelial regeneration by using light microscopy of hematoxylin and eosin survey staining.

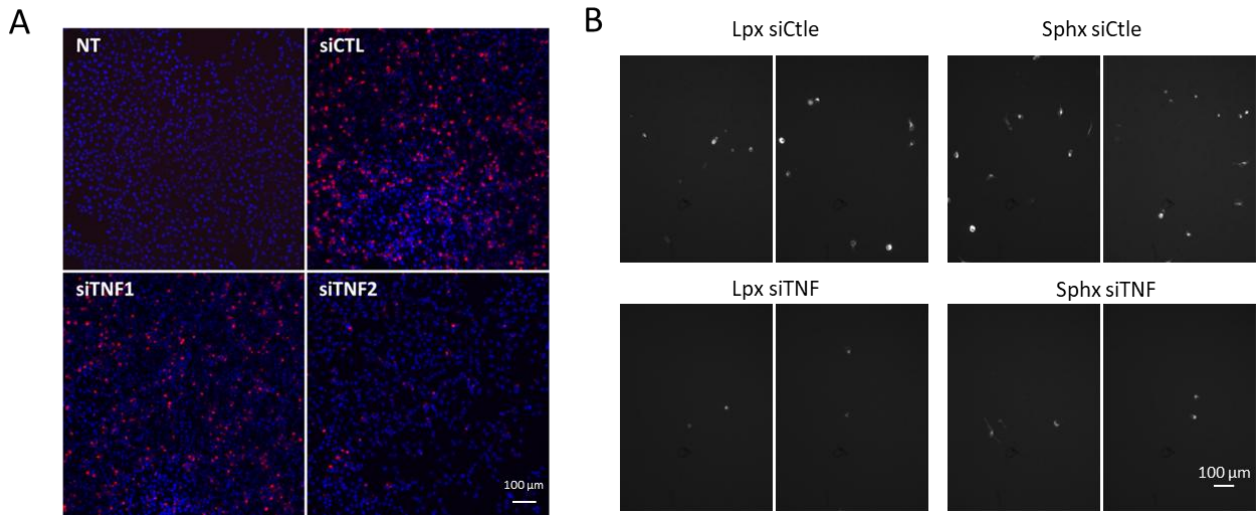

Figure S6- Validation of the gene silencing efficacy of anti-mouse TNF-α siRNAs in vitro. (A) B16 cells were transfected with lipoplexes prepared with a mixture of TNF-α coding plasmid and a siRNA specific for mouse TNF-α (sequence 1 siTNF1, or sequence 2 siTNF2) or having no target (siCTL) for 24 hours. (B) B16 cells were transfected with lipoplexes or spheroplexes prepared with a mixture of TNF-α coding plasmid and a siRNA specific for mouse TNF-α (sequence 1 siTNF1) or having no target (siCTL) for 24 hours. (A-B) At the end of the transfection, the cells were fixed with methanol, permeabilized with 0.1% Triton X-100, and the expression of TNF-α (red in A; white in B) was revealed by incubation with anti-mouse TNF-α antibody (rabbit monoclonal, Abcam ref 215188, 1/200) then with secondary anti-rabbit antibody-Alexa 594 (goat anti-rabbit IgG, Molecular Probes, ref A-11012, 1/1000), then the nuclei were stained with DAPI (blue in A, no DAPI in B). NT, non transfected cells.

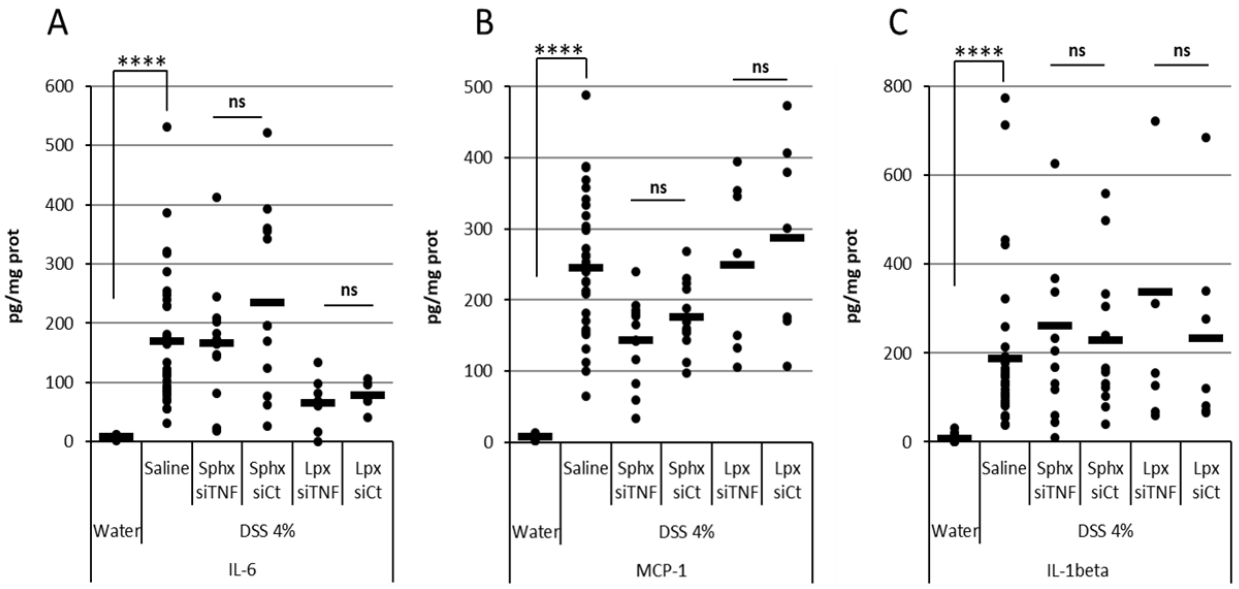

Figure S7. Assessment of *in vivo* gene silencing efficacy of Sphx and Lpx. The mice under 4% DSS in drinking water were daily orally given, from D1 to D6, Lpx or Sphx 5 prepared with siRNA anti-TNF-α (siTNF) or siRNA control (siCtl), or saline (0.9 mg siRNA/kg). On D7, the level of several cytokines, IL-6 (A), MCP-1 (B) and IL-1b (C) on a colon protein extract was evaluated by ELISA. **** $p < 0.001$. water, n=19; saline, n=32; Lpx (siTNF or siCtle), n= 7; Sphx (siTNF or siCtle), n=12).

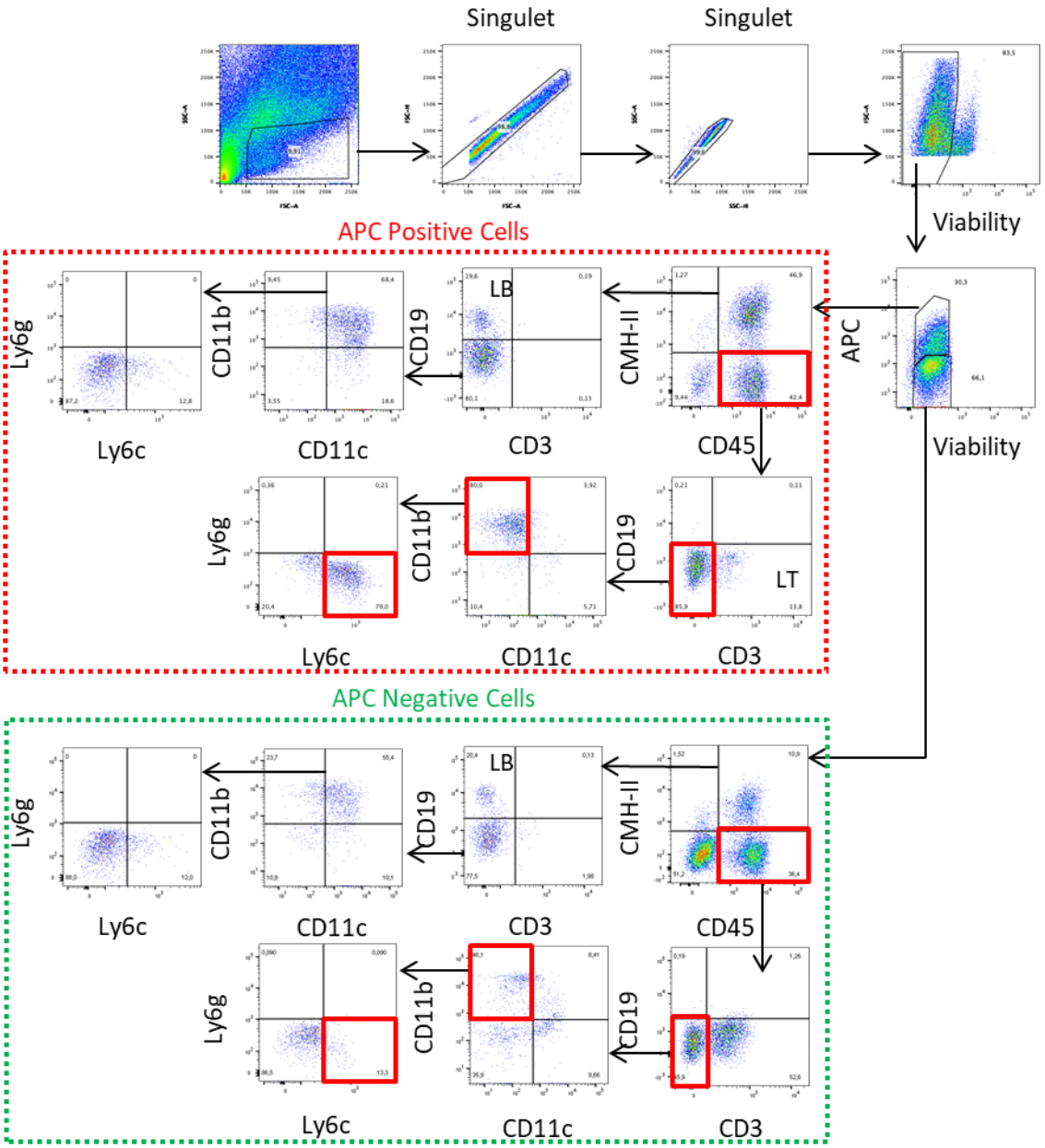

Figure S8. Gating strategy of the identification of siRNA^{+}- immune cells in the colonic mucosa by flow cytometry. The mice under 4% DSS in drinking water for 6 days were orally given Lpx or Sphx 5 prepared with fluorescent siRNA control (Alexa-647 fluorescence detected in APC channel). Colonic fragment from mice were dissociated and stained with a cocktail of antibodies making it possible to identify the T (LT) and B lymphocytes (LB) and the cells of myeloid origin. A representative experiment is given as an example.

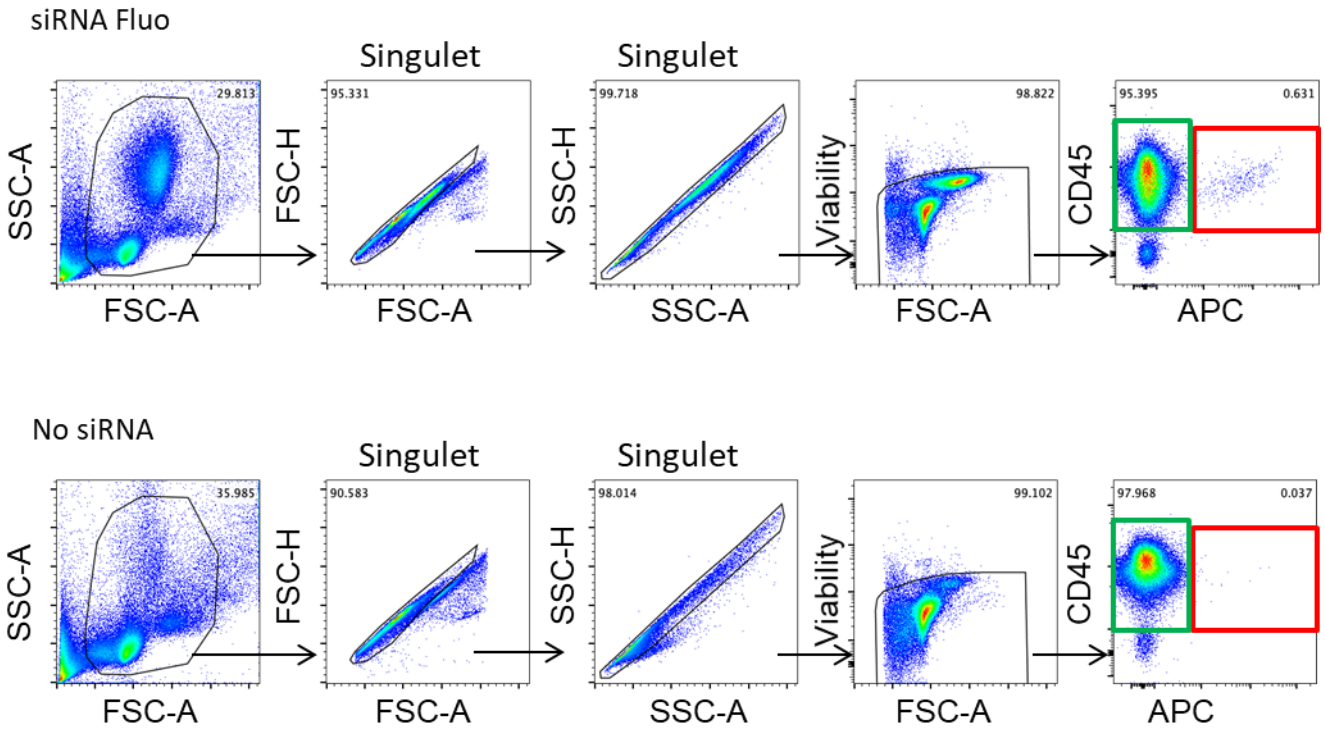

Figure S9. Gating strategy of the identification of siRNA^{+}- immune cells in blood by flow cytometry. The mice under 4% DSS in drinking water for 6 days were orally given Lpx or Sphx 5 prepared with fluorescent siRNA control (upper part, siRNA Fluo, Alexa-647 fluorescence detected in APC channel) or NaCl (lower part, no siRNA). Blood samples were collected and analysed by flow cytometry to detect cells associated with siRNA fluorescence. A representative experiment is given as an example.